



LOS ALAMOS SCIENTIFIC LABORATORY

UNIVERSITY OF CALIFORNIA
LOS ALAMOS, NEW MEXICO 87545

Telephone Ext:

OFFICE MEMORANDUM

TO : Distribution

DATE: March 30, 1979

FROM : D. W. Brown ^{7/1/79}

SUBJECT : RESULTS OF EXPT. 186, THE HIGH BACK-PRESSURE FLOW EXPERIMENT

SYMBOL : G-3/79/#4

MAIL STOP: 981

This report is being issued initially as a G-3 memorandum. It is planned to re-issue the High Back-Pressure Flow Experiment as a LAMS report near the end of April. Therefore, if you have any comments and/or additions, please have them to me in writing by April 18.

Distribution:

Greg Nunz
Rod Spence
Mort Smith
Hank Fisher
Jeff Tester
Lee Aamodt
Bob Potter
Don Brown
Jim Albright
Hugh Murphy
Chuck Grigsby

TABLE OF CONTENTS

I.	INTRODUCTION	1
	A. Objectives of Expt. 186	1
	B. General Procedure	2
	C. Time Sequence	
	D. Related Experiments	
II.	RESERVOIR THERMAL DRAWDOWN	
III.	HIGH BACK-PRESSURE RESERVOIR FLOW IMPEDANCE	
	A. Interpretation of the High Back-Pressure Flow Impedance Data	
	B. Fracture-to-Wellbore Exit Flow Impedance	
	C. Flow Shut-in Analyses: For Both Low and High Back-Pressure Flow	
	D. The Influence of Reservoir Temperature	
	E. The Apparent Reversibility of the Low Back- Pressure Flow Impedance	
IV.	EXTRAPOLATED RESERVOIR PRODUCTION RATES	
V.	GT-2B OUTLET FLOW REDISTRIBUTION DUE TO HIGH BACK- PRESSURE	
	A. Analysis of Spinner Surveys: Probable GT-2B Fracture Geometry	
	B. Flow Characterization Tracer Studies	
VI.	PERMEATION FLOW ANALYSES	
	A. Early-Time Low-Pressure Data	
	B. Early-Time High-Pressure Data	
	C. Long-Term Water Loss	
	D. Summary	
VII.	FLUID CHEMISTRY DATA	
VIII.	SUMMARY AND CONCLUSIONS	
	A. Thermal Drawdown Results	
	B. Reservoir Specific Flow Impedance	
	C. GT-2B Outlet Flow Redistribution Due to High Back-Pressure	
	D. Permeation Flow Analyses	
	E. Fluid Geochemistry	
	REFERENCES	

RESULTS OF EXPERIMENT 186, THE HIGH BACK-PRESSURE
FLOW EXPERIMENT

by

Donald W. Brown

ABSTRACT

Experiment 186, the High Back-Pressure Flow Experiment, has contributed significantly to our understanding of HDR reservoir flow processes, and pointed to a revised method of reservoir pressure management for the forthcoming 20 Mw heat extraction experiment. For the increased flow rates anticipated for this experiment -- up to 40 kg/sec -- operation in a high back-pressure flow mode may offer several advantages: lower surface injection pressures and consequently reduced water loss rates when compared to low back-pressure flow operation.

During Experiment 186, it was conclusively demonstrated that by pressurizing the exit wellbore, the reservoir flow impedance can be reduced to a very low value: about 0.4 psi/gpm. The strong implication is that at fracture exit pressurization levels close to the least principal earth stress, the high fracture-to-wellbore exit flow impedance existing under previous low back-pressure flow conditions is eliminated.

Although the hoped-for large increase in heat transfer surface was not obtained, under the somewhat higher mean pressure level existing throughout this experiment, buoyant circulation -- and therefore enhanced heat extraction -- may be occurring in the main fracture.

I. INTRODUCTION

Within the framework of the specific objectives listed below, Expt. 186, the High Back-Pressure Flow Experiment, was intended as a second long-term closed-loop reservoir drawdown experiment. Thus, Expt. 186 was similar in operation to the 75-day Phase I Heat Extraction Experiment, but with a high back-pressure imposed at GT-2, a lower initial mean reservoir temperature of 136°C, and a shorter 28-day flow duration.

A. Objectives of Expt. 186⁽¹⁾*

The first objective of this experiment was to assess the effective reservoir heat transfer surface under an imposed high back-pressure condition at GT-2. The second objective was to measure the change in the reservoir specific flow impedance caused by increasing the reservoir outlet pressure to a level close to that of the reservoir inlet, and therefore also close to S_3 .

The first experimental objective was proposed to verify a reservoir model consisting of a number of near-vertical fractures interconnected by a series of less steeply dipping joints. In theory, these near-vertical fractures in the vicinity of GT-2B would have been held closed by the earth stress during previous low back-pressure flow tests, resulting in the preferential cooling of a single more or less direct fracture connection. However, under an imposed high back-pressure at GT-2, these other fractures would tend to open and contribute significantly to the heat transfer area. This model had been proposed to explain the results of the 75-day Phase I

*Numbers in parentheses refer to the list of references at the end of this memorandum.

circulation experiment, which had indicated a permeating area considerably larger than the heat transfer area.

The second objective of this experiment was to confirm a long-held view of the author -- first indicated during Expt. 120 (May, 1976) and then exhibited again during Expt. 161 (May, 1977) -- that the reservoir specific flow impedance is controlled to a great extent by the reservoir outlet pressure level relative to the least principal earth stress, S_3 .

B. General Procedure

With GT-2 shut in, EE-1 was pressurized with the centrifugal pumps to a surface pressure of about 1300 psi, and then maintained at this level with an injection flow of about 180 gpm. When the GT-2 surface pressure reached 1400 psi, a controlled vent of GT-2 was initiated to maintain this surface pressure (\pm 25 psi). Nine hours following the initiation of pumping at EE-1, the GT-2 outflow was over 100 gpm at a back-pressure of 1380 psi -- a higher pressure than the surface pressure at EE-1 by about 100 psi. The reservoir specific flow impedance at this time was about 1.4 psi/gpm and rising as the GT-2 wellbore warmed up and the downhole fracture outlet pressure was dropping (at a constant GT-2 back pressure).

These general flow conditions were maintained for the next 28 days, interrupted only occasionally for brief shut-in periods to directly measure the buoyant pressure differential between the cold and hot legs, or to remove or replace a downhole temperature sonde. Near the end of this experiment (10-12-78), the overall specific flow impedance had dropped below 0.5 psi/gpm, with a net pressure drop across the downhole reservoir

of only 51 psi at a GT-2 outflow of 150 gpm (the surface pressure at GT-2 was still 1400 psi, 65 psi above the EE-1 surface injection pressure of 1335 psi).

C. Time Sequence

Expt. 186 formally began at 1830 h on Sept. 18, 1978 with the start of pumping at EE-1. The pumping phase of this experiment was terminated 28 days later, at 1600 h on Oct. 16. With EE-1 shut in, GT-2 was then vented for the next 7 days, until EE-1 was again repressurized at the beginning of Expt. 190 on Oct. 23, 1978.

D. Related Experiments

When relevant, the results of the experiments immediately preceding and following the High Back-Pressure Flow Experiment are reported herein. The preceding experiment, Expt. 185, was an acoustic logging experiment in GT-2 which included two pressurizations of EE-1 with GT-2 shut in⁽²⁾ The following experiment was Expt. 190, the aborted long-term pumping experiment.* In addition, numerous references are made to the results of the 75-day Phase I Heat Extraction Experiment.⁽³⁾

II. RESERVOIR THERMAL DRAWDOWN

The thermal drawdown of the fracture system connecting EE-1 and GT-2B at depth during Expt. 186 followed the same general behavior as previously exhibited during the 75-day Phase I heat extraction experiment. The single most notable difference between these two flow tests was the difference in GT-2B wellbore inflow locations. Under an imposed high back-pressure

*This experiment was originally included as the second part of Expt. 186. However, it was subsequently conducted as a separate experiment, but using the procedure as outlined in Ref. 1.

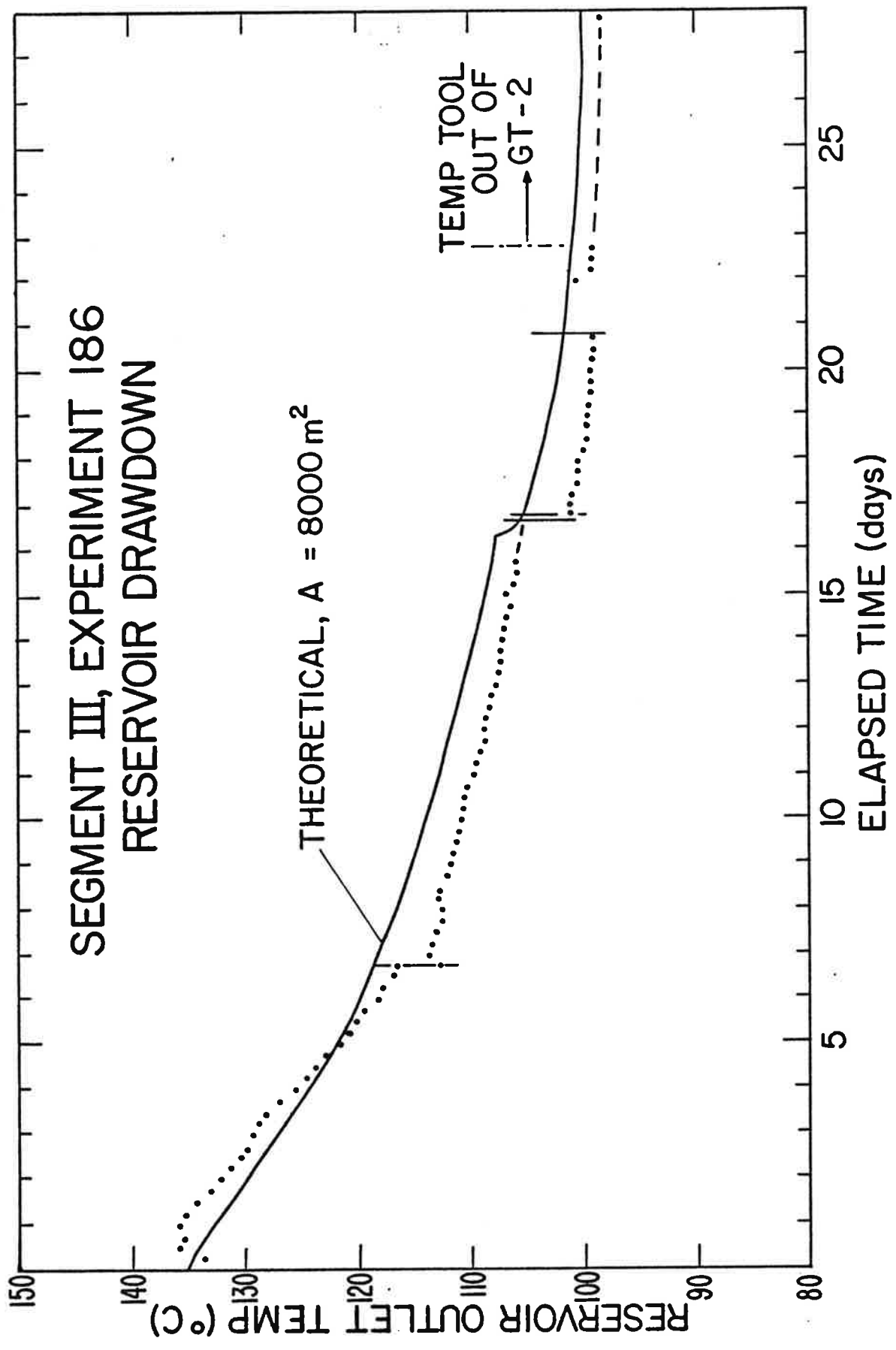
at GT-2, the majority of the fracture system flow entered the wellbore near the bottom of GT-2B, at a depth of about 8850 ft. This is contrasted to a mean entry point about 80 ft higher during the 75-day test, as discussed in a subsequent section on Flow Distribution. The effect of this change in flow distribution on the height of the effective heat transfer area, however, should have been quite noticeable, and it was not.

An effective heat transfer area (one side of the fracture) of 8000 m^2 was again found to match the reservoir drawdown data, as shown in Fig. 1. Since this is the same area as for the previous 75-day test, we must conclude that operation in the high back-pressure mode did not result in the hoped for large increase in heat extraction area.

However, under conditions of high back-pressure at GT-2, the height of the directly-connected flow path between EE-1 and GT-2B decreased by about 25% relative to the 75-day flow test. Given that the majority of the flow exits the EE-1 wellbore at a depth of 9050 feet, the major fracture exit point (69% of the total flow) at 8850 feet during Expt. 186 results in an effective decrease in reservoir height from 310 feet to only about 230 feet.

However, as shown in Fig. 1, the theoretical curve representing the drawdown of a 8000 m^2 fracture matches the measured drawdown performance quite well. The tentative conclusion is that natural convective circulation in the fracture under conditions of high overall fracture pressurization is compensating for this 25% loss in directly-connected fracture height. This conclusion would not obtain if the deeper wellbore connections in GT-2B represented more tortuous flow connections, but other data strongly deny

Figure 1



this possibility. The bromine tracer test (Expt. 193) performed after Expt. 186 shows that the wellbore entrance points near the bottom of GT-2B (at about 8650 feet) represent the shortest and most direct connections to EE-1.⁽⁴⁾

Some speculative calculations based upon the impedance of the main fracture (wellbore-to-fracture impedances excluded) suggest that the aperture of the main fracture connection is of the order of 0.5 mm. This fracture opening is sufficient to yield a buoyancy parameter of 1, i.e. natural convection equals viscous drag in magnitude.

One curious artifact of high back-pressure flow operation has not been explained, however. Prior to Expt. 186, several low-flow low back-pressure tests indicated a mean recovered reservoir surface temperature of only 130°C. However, during the first day of Expt. 186, the reservoir outlet temperature was above 135°C. One possible explanation for this phenomenon is that natural convection in the initially inflated fracture system under high back-pressure operation augmented the previously-available fracture area under the earlier low back-pressure flowing conditions.

The fracture system thermal performance data are given in Table I. As shown, the reservoir thermal power dropped only slightly during the majority of Expt. 186 because the flow rate increased to compensate for the thermal drawdown.

TABLE I

Thermal Performance Data, Expt. 186

Day:	<u>1</u>	<u>24</u>
Outlet Flow Rate, gpm	100	150
Reservoir Inlet Temp., °C	74	61
Reservoir Outlet Temp., °C	135	99
Thermal Power, MW	1.54	1.44

III. HIGH BACK-PRESSURE RESERVOIR FLOW IMPEDANCE

The most significant result of Expt. 186 was the clear demonstration that the reservoir specific flow impedance, except for the small and essentially constant inlet flow impedance, is a function of the reservoir outlet pressure. The majority of the fracture flow impedance is concentrated near the fracture outlet, and appears to be controlled by the effective fracture closure stress (ΔP_c) at this location as discussed in Section III below. For a wellbore fluid pressure at the fracture intersection with the wellbore equal to P_w , and the least principal earth stress at this depth being S_3 ,

$$\Delta P_c = S_3 - P_w$$

A. Interpretation of the High Back-Pressure Flow Impedance Data

Initially, the overall reservoir specific flow impedance was plotted vs time in the usual manner (several earlier curves of this form were presented at Expt. 186 briefing sessions). However, when the early time data

were added to this curve, an unusual variation was noted, as seen in Fig. 2. During the first five days of this experiment, the impedance first increased from its initial value of about 1.3 psi/gpm to a maximum value of 2 psi/gpm, and then dropped quite sharply again to a value of about 1.3 psi/gpm.

During this same time as shown in Fig. 1, the reservoir outlet temperature initially rose by about 2°C to a level of 136°C after 12 hours, and then remained essentially constant at this value for the next 18 hours (the specific impedance was still rapidly increasing at 12 hours, as shown in Fig. 2). The fracture outlet temperature then dropped considerably to about 122°C at the end of five days. Obviously then, the reservoir specific impedance was not following the fracture outlet temperature variation, but still appeared to be somehow related to temperature. However, it was the mean GT-2 wellbore fluid temperature that it was responding to: first rising sharply as the warm fluid in the fracture system filled the GT-2 wellbore, and then dropping again as the reservoir was cooled by continued flow into EE-1.

Since the quantity effected by variations in the temperature of the fluid column in GT-2 (at a constant surface pressure) is the downhole pressure, the Expt. 186 specific impedance data were replotted vs reservoir pressure, as shown in Fig. 3. As can be seen, a remarkably good correlation results, with a RMS deviation of about ± 20 psi in the linear fit (the data scatter is emphasized by the scale of this plot). These results reconfirm the conclusion drawn from a re-analysis of the Expt. 161 data taken during the flow testing of the EE-1/GT-2A fracture connection: that the reservoir flow impedance is primarily a function of the fracture outlet pressure level relative to S_3 .⁽⁵⁾

Figure 2

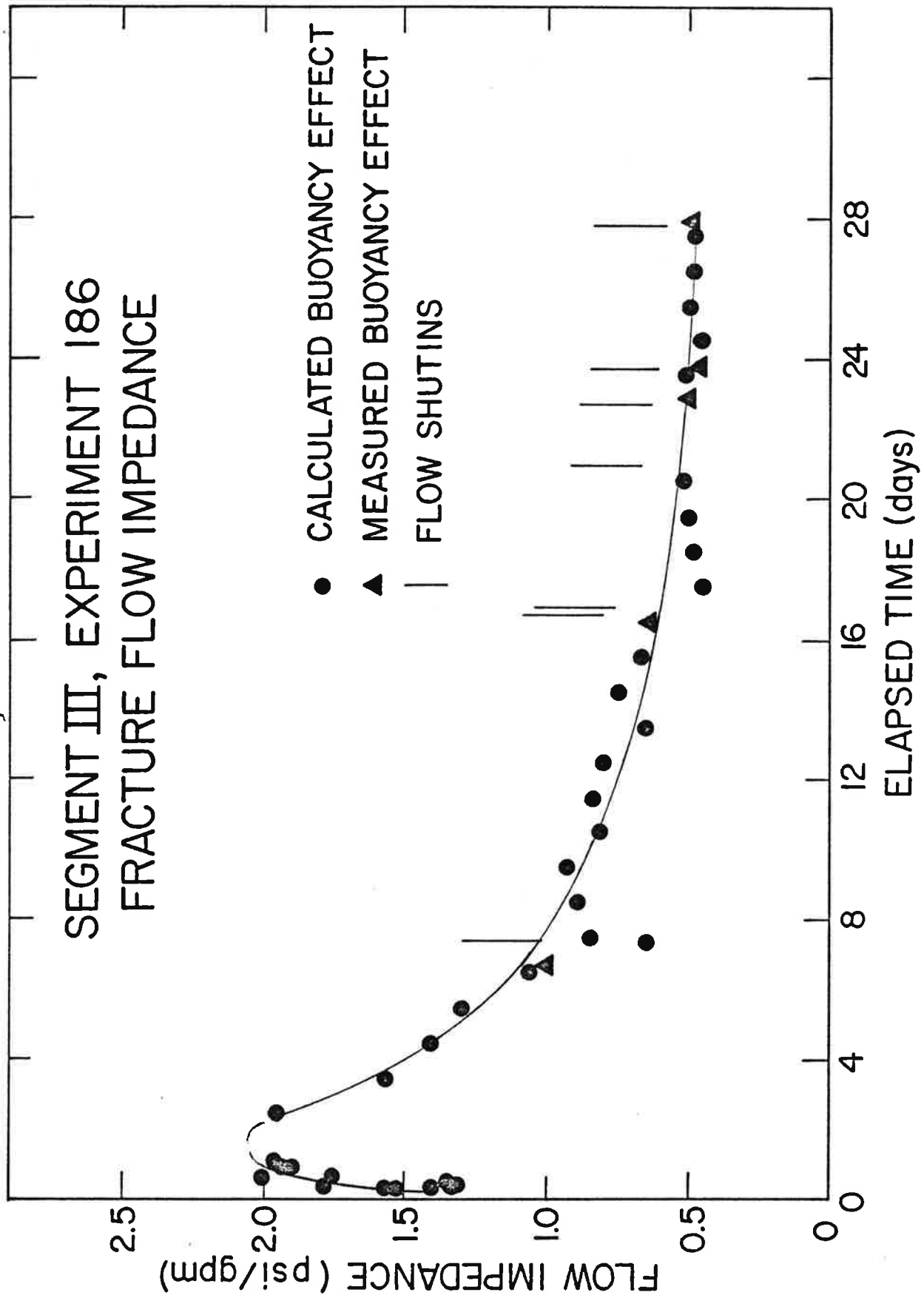
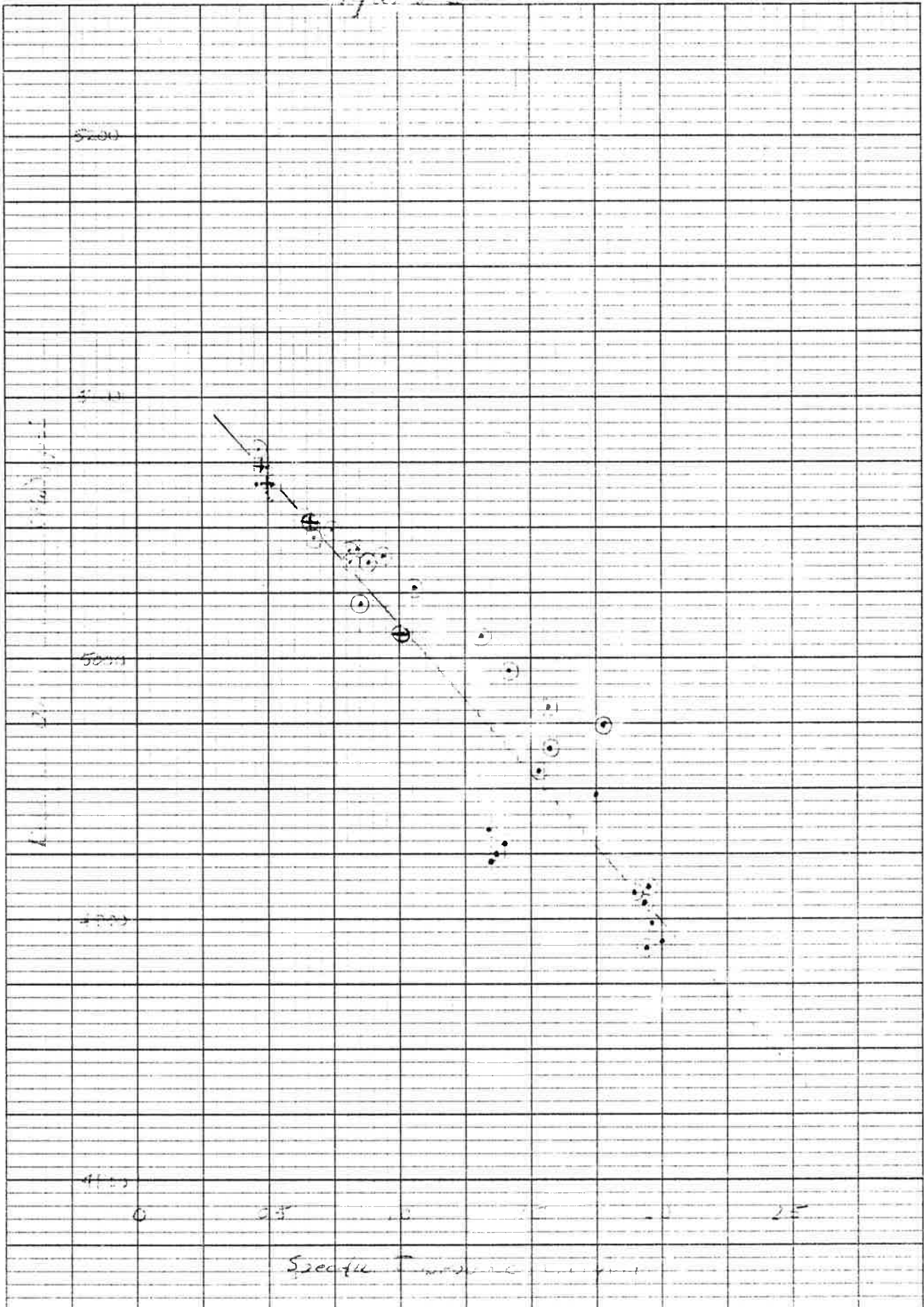


Figure 2



SQUARE 5 X 5 TO THE HALF INCH AS 0811-00

5 COLUMBIAN UNIVERSITY LIBRARY 1000 UNIVERSITY AVENUE NEW YORK, N.Y. 10003

B. Fracture-to-Wellbore Exit Flow Impedance

However, Fig. 3 shows the overall reservoir specific flow impedance, including the near-constant EE-1 wellbore-to-fracture inlet impedance and both wellbore pressure drops. If only the flow shut-in buoyancy calibration data are analyzed, the measured GT-2B near-wellbore fracture impedance (fracture-to-wellbore) can be obtained from the initial pressure rise at GT-2, by subtracting out the small calculated wellbore pressure drop. These data are plotted in Fig. 4. This figure reveals several important things. First, the fracture outlet impedance appears to vanish at a downhole pressure of 5090 psi,* herein interpreted as the fracture opening pressure (S_3 for a near-vertical fracture) at a depth of 8850 feet. Second, when compared to Fig. 3, a residual -- and supposedly minimum -- overall fracture system flow impedance of 0.4 psi/gpm would have been obtainable for the flow conditions of Expt. 186.

C. Flow Shut-in Analyses: For Both Low and High Back-Pressure Flow

From a careful examination of the surface pressure responses at EE-1 and GT-2 during flow shut-ins, the several components of the overall fracture flow impedance can be recognized. The instantaneous pressure responses at EE-1 and GT-2 represent the localized fracture inlet and outlet flow impedances.** The longer-term pressure responses at EE-1 and GT-2 -- which finally stabilize to give a direct measure of the buoyant ΔP -- give an indication of the distributed flow impedance along the fracture itself.

Figures 5 and 6 show two flow shut-ins near the end of Expt. 186 which were used to measure the buoyant ΔP . The shapes of both these sets of shut-in curves, with the abrupt pressure drops at EE-1 and the almost as abrupt

*Corresponding to a GT-2 surface pressure of 1420 psi near the end of Expt. 186.

**The small casing friction pressure drops must first be calculated, and then subtracted from these instantaneous shut-in pressure responses to actually obtain the inlet and outlet flow impedances.

Fig =

SQUARE 5 X 5 TO THE HALF INCH AS-0811 6H

Standard Oil Company (Indiana) - Standard Oil Company - Standard Oil Company

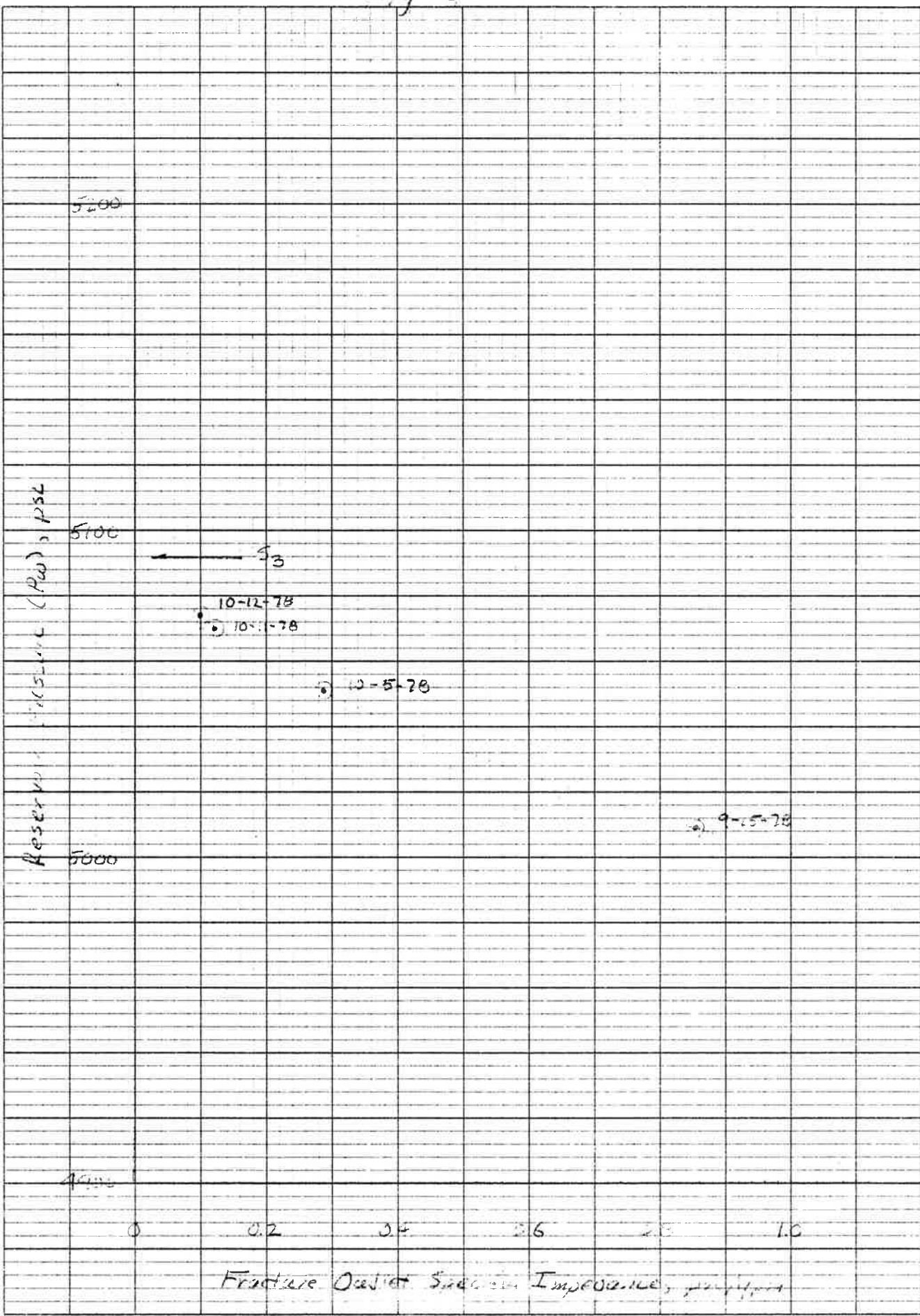


Figure 5

1450

10-15-78 Sunday

Well Fracture $\Delta P = 1370 - 70 = 1300$ psi

Outlet $\Delta P = 23$ psi

Inlet $\Delta P = 35$ psi

Fracture $\Delta P = 52$ psi

23 psi

1400

65

70 psi
back pressure

Fracture ΔP

1370 psi

Pressure, psi

1350

$k_{eff} = 1.91 \times 10^{-1}$

35 psi

85-1

1300

1700

1715

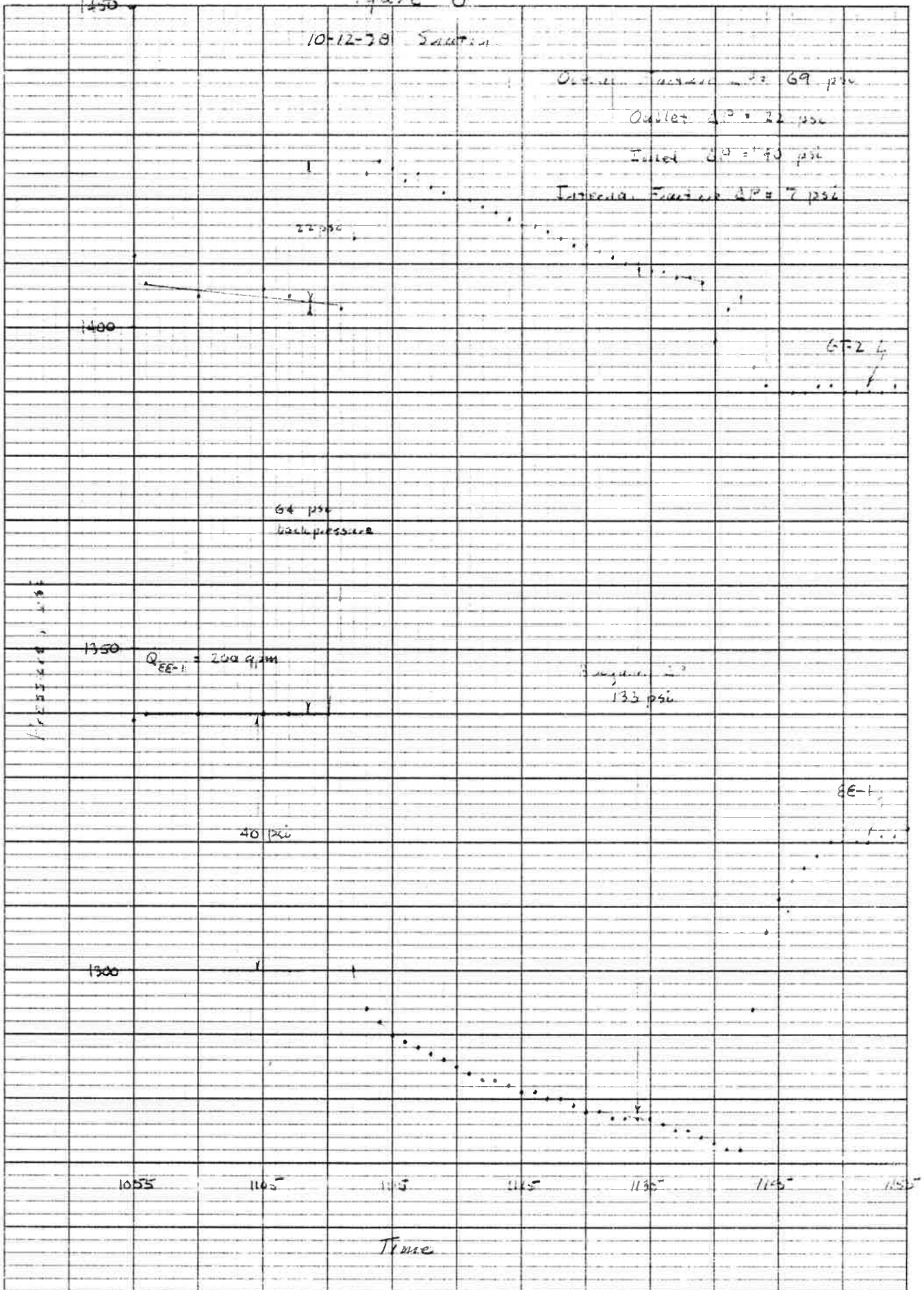
1730

1745

1750

Time

Figure 6



pressure increases at GT-2, strongly imply that the majority of the fracture system flow impedance is concentrated near the fracture inlet and exit points. For both of the high back-pressure flow shutins shown, the outlet impedance is the lower: when corrected for the small GT-2 casing friction loss, about 0.1 psi/gpm.

The remainder of the flow impedance, which is distributed along the fracture itself, is negligibly small: less than 10 psi in both cases (at a flow rate of about 150 gpm). Therefore, with the fracture system pressurized from both ends at a pressure level close to S_3 , the internal flow impedance of the fracture itself almost vanishes, i.e. the fracture must be essentially inflated.

Similar analyses of the flow shutins at the end of the 75-day Phase I flow test and during Expt. 190 result in a rather remarkable -- but irrefutable -- conclusion: In a low back-pressure flow mode, almost all of the reservoir flow impedance is concentrated near the fracture exit. This high GT-2 fracture-to-wellbore flow impedance is most probably a direct consequence of the wellbore stress concentration, since this same impedance almost completely vanishes with a high back-pressure at GT-2, as clearly demonstrated during Expt. 186.

Figure 7 shows the Phase I flow shutin data upon which these conclusions were based. As can be seen, following the flow shutin of GT-2, there was an almost instantaneous pressure rise of about 635*psi at GT-2, representing a low back-pressure fracture-to-wellbore exit flow impedance of 2.6 psi/gpm. The corresponding flow shutin at EE-1 resulted in a 58 psi pressure drop. When corrected for casing friction losses, this corresponds to an EE-1

*623 psi when corrected for the casing pressure drop.

wellbore-to-fracture inlet flow impedance of 0.18, almost identical to that measured during Expt. 186. The longer-term pressure recovery data at EE-1 and GT-2 indicate a distributed fracture impedance of about 0.18 psi/gpm, at a mean fracture pressurization level of about 800 psi.

The shutin flow data during Expt. 190, the low back-pressure long-duration flow test following Expt. 186 (which was aborted after only four days) also support the above conclusions concerning the concentration of low back-pressure flow impedance near the fracture exit. The surface pressure responses at EE-1 and GT-2 during this short (22 minute) flow shutin are shown in Fig. 8. Again, there is an essentially instantaneous pressure rise at GT-2 of 1160 psi, representing a fracture-to-wellbore exit flow impedance of 5.2 psi/gpm -- the majority of the overall 5.65 psi/gpm fracture system flow impedance at this time. The 72 psi pressure drop resulting from the shutin at EE-1, when corrected for casing friction losses, corresponds to a 0.16 psi/gpm wellbore-to-fracture inlet flow impedance, very close to other measurements. However, the longer-term pressure recovery data EE-1 and GT-2, at this higher mean reservoir pressurization level of about 1200 psi (and closer to S_3) show a lower distributed fracture pressure drop of about 30 psi, as would be expected. The corresponding distributed fracture impedance at this higher fracture pressurization level is only 0.13 psi/gpm.

D. The Influence of Reservoir Temperature

The question now to be asked is what phenomenon, in the absence of significant wellbore pressurization at GT-2, produced the significant decrease in reservoir specific impedance during the 75-day Phase I test? From an early value of about 15 psi/gpm, the reservoir specific impedance slowly decreased during this test to a final value of about 3 psi/gpm.

Since the majority of this impedance is undoubtedly concentrated near the fracture exit at GT-2B, the variation in this impedance (at a low and near constant GT-2 wellbore pressurization level) must have been caused by the variation in an analog of pressure. Crossplotting the specific impedance and reservoir exit temperature profiles from the 75-day flow test, as suggested by Hugh Murphy, gives the answer: The thermal-cooldown-induced stresses near the fracture exit at GT-2B -- a direct analog of pressure -- probably accounted for the observed decrease in fracture flow impedance during this test.* The plot of reservoir exit temperature vs. flow impedance is shown in Fig. 9. As can be seen, following the initial reservoir transient flow interval, there appears to be a remarkably good correlation between reservoir outlet temperature and flow impedance.

E. The Apparent Reversibility of the Low Back-Pressure Flow Impedance

One final point needs to be made regarding the fracture system flow impedance under low back-pressure conditions at GT-2. Although Expt. 190 was terminated after only 4 days due to flow bypass at EE-1, it was sufficiently long to again measure the reservoir flow impedance, as previously mentioned. On 10-25-78, just prior to a flow shutin where the buoyancy was measured, the following conditions obtained:

EE-1 Pressure and Flow: 1325 psi at 308 gpm

GT-2 Pressure and Flow: 214 psi at 224 gpm

Buoyant ΔP (Measured): 153 psi

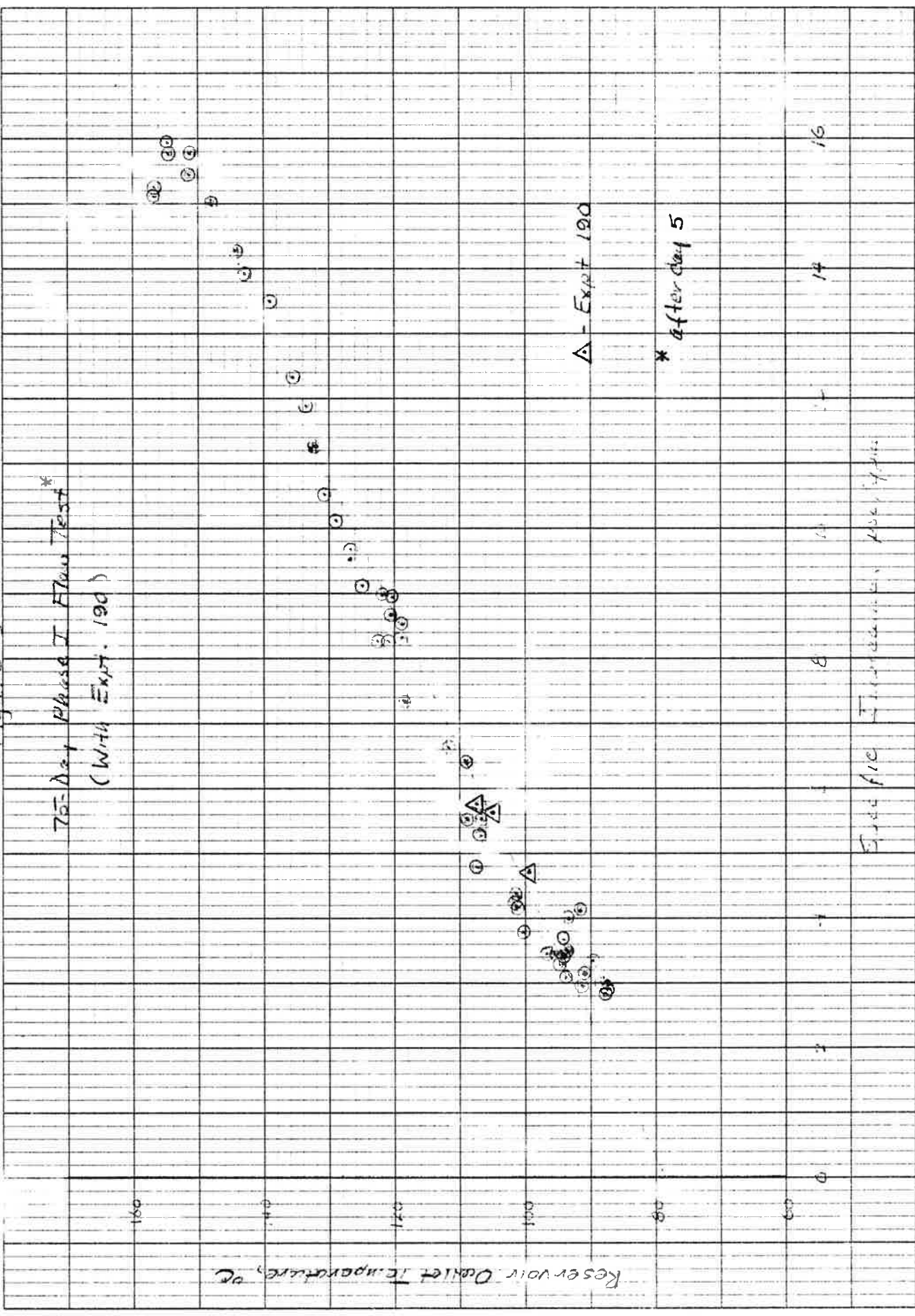
Reservoir Outlet Temperature: 105°C

For these above conditions, the total reservoir specific impedance had markedly increased again (from that during Expt. 186) to a value of 5.65 psi/gpm, as also shown in Fig. 9.

*Although not pursued here, a future study will attempt to correlate the reservoir outlet temperature at which this impedance essentially vanishes (about 80°C) with the calculated stress field -- including the effects of thermal stress -- near the wellbore. A possible result of this study would be an effective in-situ Young's Modulus for the rock mass.

Figure 9

75-Day Phase I Flow Test*
(With Expt. 190)



△ - Expt 190

* After day 5

Specific Instructions: Ask for this

Further, and most important, this value is almost identical to the reservoir specific impedance of 5.6 psi/gpm measured on the 36th day of the 75-day Phase I test, at almost exactly the same reservoir outlet temperature level (106°C). The obvious conclusion is that the low back-pressure fracture flow impedance is reversible. The observed decrease in reservoir specific impedance during Phase I was probably not due to a continuing state of fracture movement, but rather to a continued cooling of the rock near the reservoir exit.

In addition, the obvious should be pointed out: A reduction in reservoir specific flow impedance produced by drastically cooling the reservoir exit region is a very non-productive approach to reservoir management for our program.*

IV. EXTRAPOLATED RESERVOIR PRODUCTION RATES

It has been said that the reservoir back-pressure condition really doesn't make much difference, since the observed flow rates under low and high back-pressure flow were roughly the same. However, with a limited long-term EE-1 pressurization capability (and below S_3), it is apparent that this comparison is not really valid. With a net reservoir ΔP of only about 60 psi near the end of Expt. 186, an increase of 70 psi at EE-1, from 1330 psi to 1400 psi, would probably have doubled the GT-2 outflow rate. Unfortunately, our centrifugal pumps are not capable of delivering 300 gpm at a wellhead pressure of 1400 psi, so this point could not be demonstrated.

In Ref. 6, J. Tester et al discuss the economics of HDR geothermal systems in considerable detail. In this report, the minimum reservoir flow rate considered is 40 kg/sec (633 gpm). It is an illuminating exercise to

*The Phase I low back-pressure specific flow impedance was only reduced to the marginally acceptable value of 3 psi/gpm after an excessive cooling of the reservoir outlet region to below 90°C, a rather non-productive outlet temperature level for a HDR reservoir.

extrapolate the flow performance of our present reservoir* to a reservoir flow rate of only 500 gpm (31.6 kg/sec). For this flow condition, only one reservoir outlet temperature was selected: 99°C. This is a temperature for which the buoyancy ΔP is known, and for which the repeatability of the low back-pressure reservoir specific flow impedance shown in Fig. 9 cannot be disputed.# The required surface pressures and supporting information are given in Table II. From Table II one can infer several things. First, as discussed in Section III above, with most of the pressure drop concentrated at the GT-2 fracture outlet, the water loss rate would be higher under low back-pressure flow conditions. Second, the overall reservoir pressure requirements would be reduced, and with a considerable reduction in power requirements, under a high back-pressure flow condition,

TABLE II
FLOW CONDITIONS AT A 500 GPM RESERVOIR
FLOW RATE ($T_{out} = 99^{\circ}C$)

	<u>High Back-Pressure</u>	<u>Low Back-Pressure</u>
Buoyant ΔP , psi	133	133
GT-2 Surface Pressure, psi	1470	200
Overall Specific Impedance, psi/gpm	0.47	4.4
EE-1 Surface Pressure, psi	1570	2270
Pumping Power, Kw	10	200

*The one connecting EE-1 and GT-2B prior to remedial casing cementing operations in January, 1979.

#Besides, a comparison at a more reasonable reservoir outlet temperature of 150°C (15 psi/gpm from Fig. 9) would have been an exercise in futility!

V. GT-2B OUTLET FLOW REDISTRIBUTION DUE TO HIGH BACK-PRESSURE

A. Analysis of Spinner Surveys: Probable GT-2B Fracture Geometry

Spinner surveys of the open-hole section of GT-2B, intended to measure the distribution of flow between the several wellbore fluid entry points, were taken before, during, and after the high back-pressure experiment. The pre-Expt. 186 spinner survey was taken on 4-12-78, one day before the termination of the 75-day Phase I flow test.⁽⁷⁾ The Expt. 186 spinner survey was conducted on 10-12-78, coincident with a flow shutin four days before the end of this experiment. The post-Expt. 186 spinner survey was taken on 11-1-78, following Expt. 190.

The results of these three spinner surveys are shown in Fig. 10. As can be seen, the two low back-pressure flow distribution curves are generally similar, but considerably different from the high back-pressure flow distribution curve. Since much of the following discussion will be directed at the lowermost wellbore fracture connections shown in Fig. 10 (at a median depth of approximately 8850 feet), a tentative conclusion needs to be made now, and supported later. This conclusion is that these two lowermost points of fluid entry, separated by only about 20 feet, are in fact a single near-vertical fracture,* with the majority of the flow being concentrated at the two ends of the very elongated elliptical fracture intersection with the steeply-dipping GT-2B wellbore, as illustrated in Fig. 11. The fact is, as we have often seen in core samples containing very steeply dipping fractures, the majority of the drilling-related mechanical damage to these exposed fractures (chipping, erosion and abrasion) has been concentrated at the thin, tightly-curved and vulnerable ends of these elliptical fracture intersections with the core. Further,

*Within 2 or 3 degrees of vertical.

Figure 10

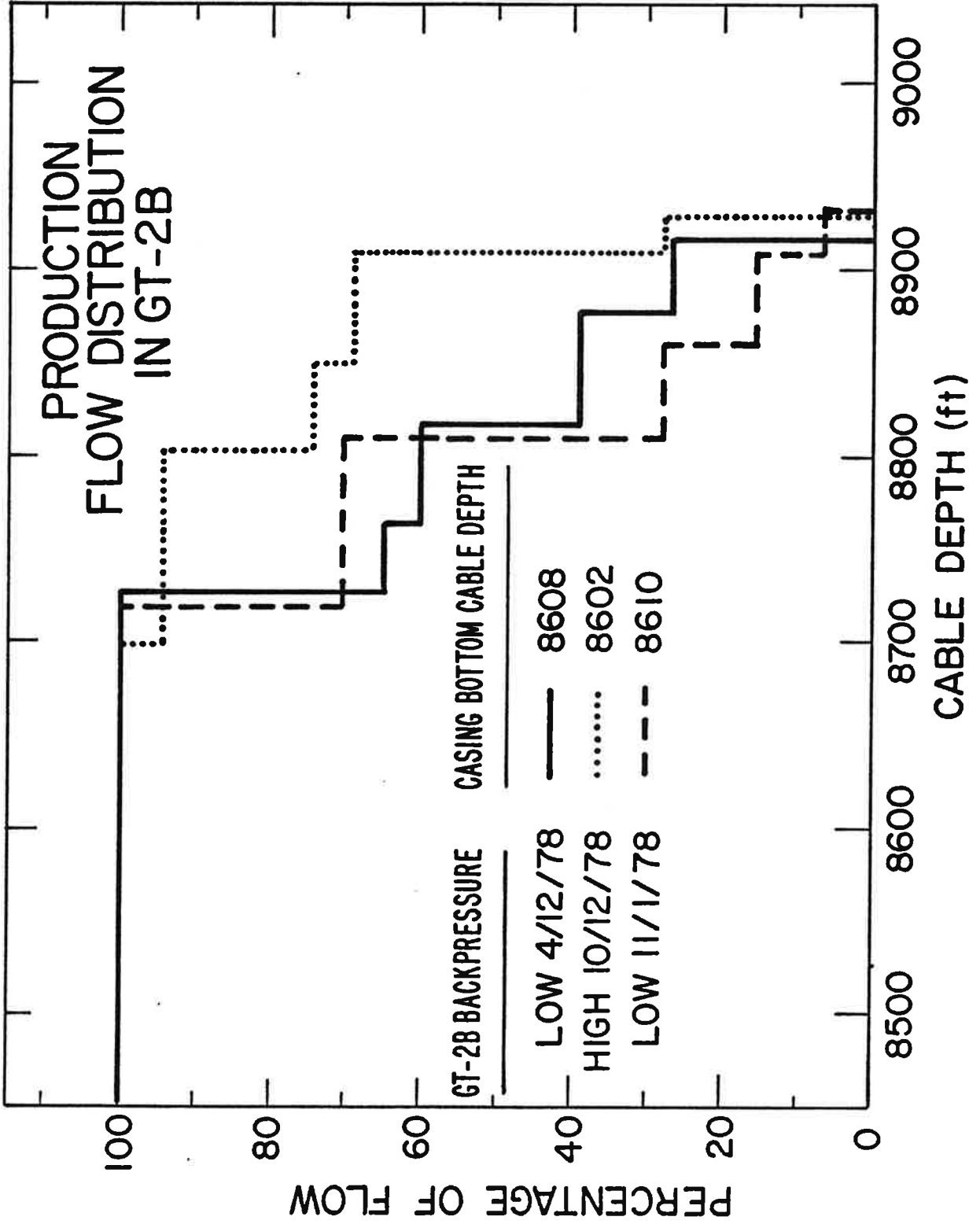
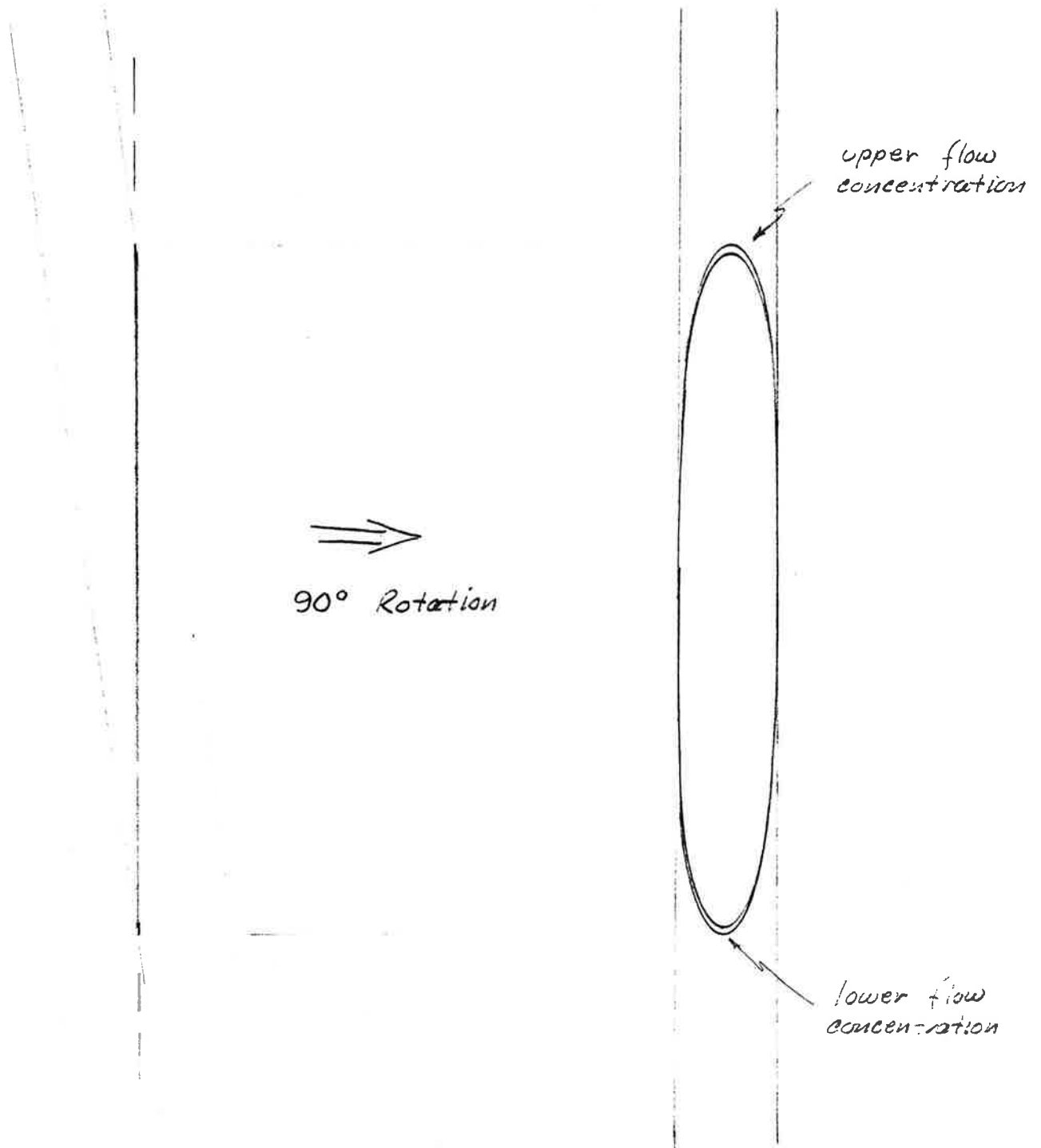


Figure 11

Schematic Representation of the Intersection
of a Near-Vertical Fracture With the G.T.-23
Wellbore at the 8850-foot Depth



a near vertical fracture intersection with the 10-inch diameter GT-2B wellbore, inclined from the vertical by about 4° at this depth, could have a wellbore exposure close to 20 feet high, depending on the difference in azimuth between the wellbore direction and the fracture direction.

Table III lists, for the three spinner surveys shown in Fig. 10, the depth to the flow-weighted mean point of fluid entry into the GT-2B wellbore.

TABLE III
SPINNER SURVEY DATA FOR GT-2B

<u>Survey Date</u>	<u>GT-2 Back-Pressure Flow Condition</u>	<u>Mean Fluid Entry Point, ft</u>
4-12-78	Low	8736
10-12-78	High	8822
11-1-78	Low	8741

Table IV summarizes the relevant flow data associated with the first two spinner surveys listed in Table III.*

TABLE IV
SPINNER-SURVEY-RELATED FLOW DATA

<u>Survey Date & (Condition)</u>	<u>Total GT-2 Outlet Flow, gpm</u>	<u>Flow Through 8850-ft Fracture Connection, gpm</u>	<u>Total Reservoir ΔP, psi</u>	<u>Fracture-to-wellbore ΔP, psi[#]</u>
4-12-78 (low)	242	63 (26%)	728	623
10-12-78 (high)	149	103 (69%)	65	18
11-1-78 (low)	--	(16%)	--	--

*Flow data are not listed for the post Expt. 186 spinner survey, since no acceptable steady-state flow condition was established during this rather short flow test.

[#]These fracture-to-wellbore ΔP values were obtained from the associated flow shutin data discussed earlier, by subtracting out the small casing friction loss (see Figs. 6 and 7).

The data of Tables III and IV illustrate that under an imposed high back-pressure condition at GT-2, the mean wellbore fluid entry point is deeper by 80 to 85 feet than under low back-pressure flow conditions. Another significant feature of these flow distributions is their reversibility, as also shown in Fig. 10. The major flow connection near the bottom of GT-2B that markedly opened under high back-pressure flow conditions, closed again when the back-pressure was reduced to the previous 200 psi level of the 75-day test.

Of even more significance is the fact that during Expt. 186, more total flow was exiting through this lowermost fracture connection, but under a very much reduced driving ΔP , as shown in Table IV. . By selecting the appropriate flow model (either laminar or turbulent), one can calculate the change in fracture permeability between the low and high back-pressure flow conditions listed in this table. For a representative fracture height of 20 feet, but with the flow concentrated at the two ends of the very elongated elliptical fracture-wellbore intersection as depicted in Fig. 11, an appropriate Reynold's number for the flow would be in the range of 2000. Therefore, a turbulent flow model would be the more appropriate for flow across this fracture-to-wellbore impedance.

The change in fracture permeability under turbulent flow conditions can be represented as:*

$$\frac{K_h}{K_\ell} = \frac{\dot{Q}_h}{\dot{Q}_\ell} \sqrt{\frac{\Delta P_\ell}{\Delta P_h}} \quad (1)$$

*h \rightarrow high back-pressure, $\ell \rightarrow$ low back-pressure; k = permeability.

For the data listed in Table IV,

$$\frac{K_h}{K_\ell} = \frac{103}{63} \sqrt{\frac{623}{18}} = 9.8$$

The above pressure-induced change in the measured fracture permeability can be compared to experimental fracture permeability variations with confining pressure (or stress) reported in the literature. In Ref. 8, a laboratory study of the effect of confining pressure on fracture permeability for low porosity rocks, the following empirical equation was developed:

$$\left(\frac{K_1}{K_2}\right)^{1/3} = \frac{\log P_1 - 4.602}{\log P_2 - 4.602} \quad (2)$$

where $P = \text{Net Confining Stress, } S_3 - P_\omega$

Taking the value for S_3 of 5090 psi as shown in Fig. 4, and the value for P_ω corresponding to the 10-12-78 flow shutin data for which the Table IV values were developed, a net fracture confining stress of only 20 psi (P_h) at high back-pressure results. For the same value of S_3 , the terminal flow shutin data from the 75-day test result in a low back-pressure net fracture confining stress of 1210 psi (P_ℓ).

For these values of P_h and P_ℓ , equation (2) gives:

$$\frac{K_h}{K_\ell} = \left[\frac{\log (20) - 4.602}{\log (1210) - 4.602} \right]^3 = 10.7$$

Obviously, there is remarkable agreement between our in-situ fracture flow measurements and the extensive laboratory flow tests reported in Ref.8. In fact, the somewhat lower value for the in-situ permeability difference

given by equation (1) may be due to the 11°C difference in the GT-2B near-wellbore reservoir rock temperature between the two measurements listed in Table IV. *

One nagging problem remains, however, in the above development. Suppose this fracture intersection at 8850 feet in GT-2B is not vertical, but is instead a high-angle joint (or two) dipping at 70° from the horizontal. # Then the S_3 value used above to calculate the net fracture confining stress is not appropriate. For an S_3 value of 5090 psi as given above, and for an S_1 value of 9770 psi (equal to ρgh at a depth of 8850 ft, for $\rho=2.6$ gm/cc), the stress normal to a joint dipping 70° between S_1 and S_3 would be:

$$S_n = S_1 \sin^2\theta + S_3 \cos^2\theta \quad (3)$$

$$\text{where } \theta = 90^\circ - 70^\circ = 20^\circ$$

$$S_n = 1143 + 4495 = 5638 \text{ psi}$$

or

$$S_n = S_3 + 548 \text{ psi}$$

In this case, P_h would equal 568 psi and P_x would equal 1758 psi. Using equation (2), the predicted variation in the permeability of a 70°-dipping joint, between the low and high back-pressure conditions given in Table IV would be:

*At the end of the 75-day flow test, the reservoir outlet temperature was 88°C, while on 10-12-78 during Expt. 186, the reservoir outlet temperature was 99°C.

#An angle which is very representative of the joints observed in core samples and televiewer scans of the GT-2 wellbore.

$$\frac{K_h}{K_\ell} = \left[\frac{\log(568) - 4.602}{\log(1758) - 4.602} \right]^3 = 2.5$$

This variation is obviously much less than the observed permeability variation between low and high back-pressure conditions at GT-2, strongly supporting the conclusion reached earlier: That the lowermost flow connection in GT-2B is the intersection of a near-vertical fracture with the wellbore.

But, can we say anything about the other flow connections in GT-2B? If one assumes that all the other flow connections in GT-2B represent the intersections of high-angle joints with the wellbore, one can use equation (1) to compare the measured in-situ permeability variation between low and high back-pressure flow conditions for these joints with that predicted by equation (2). The low back-pressure and high back-pressure flow residuals assigned to these combined joint intersections with the GT-2 wellbore are from Table IV:

$$\dot{Q}_h = 149 - 103 = 46 \text{ gpm}$$

$$\dot{Q}_\ell = 242 - 63 = 179 \text{ gpm}$$

From equation (1)

$$\frac{K_h}{K_\ell} = \frac{46}{179} \sqrt{\frac{623}{18}} = 1.5$$

In comparison, the predicted joint permeability variation between low and high back-pressure flow, using equation (2) is 2.5 for a joint dipping 70° as given above, and 1.3 for a joint dipping at 65°.

Obviously, then, the following GT-2B flow connection model fits the observed data:

- A lowermost near-vertical fracture-wellbore intersection centered at a depth of about 8850 feet.
- A set of high-angle joints, dipping between 65 and 70 degrees, which intersect the wellbore between the depths of 8660 feet and 8800 feet.

B. Flow Characterization Tracer Studies

Two dye tracer experiments (1-5 and 1-6) were conducted during Expt. 186. The results of these experiments are compared with the low back pressure tracer experiments run at the end of the 75-day test (1-4, 4/7/78), and following the high back pressure experiment, during Expt. 190 (1-7, 10/26/78). Table V and Figs. 12-17 illustrate the results.

In all cases, a Na-fluorescein tracer was injected at the EE-1 wellhead. Test 1-4 used the Kobe system for this while all subsequent tests used the new dye injection by-pass system at EE-1. After injection, the dye slug was pumped down EE-1, through the fracture system, and recovered at the GT-2 wellhead. Although tracer tests conducted under low and high back pressure conditions at GT-2 showed a well-mixed, highly dispersed residence time distribution with mean fracture system volumes in excess of 7000 gal, there are some prominent differences:

- (1) The early high back-pressure test (1-5, 9/28/78) showed an initial arrival of dye at a residence time that would correspond to something less than the EE-1 and GT-2 wellbore volumes based on flow-rate weighted averages of the injection and production zones volumes,

TABLE V

Dye Tracer Experiments During Phase 1

<u>Experiments</u>	P_{GT-2} psi	q_{GT-2} gpm	Mean <V> gal	Median [V] gal	Variance σ^2_{θ}	Peak dye Concentration ppm	Dye re- covery %	<u>Comments</u>
1-4 (4/7/78)	200	245	14854	12787	0.465	(0.78) ^a	> 60	~3 gpm water loss
1-5 (9/28/78)	1400	122	7713	5493	0.958	1.80	60	~50 gpm combined annulus leak and water loss.
1-6 (10/13/78)	1400	148	12997	10338	0.599	1.36	74	~50 gpm combined annulus leak and water loss
1-7 (10/26/78)	250	248	13106	10712	0.487	0.60	33 ^b	~68 gpm combined annulus leak and water loss

(a) Corrected to correspond to the feed concentration used in 1-5, 1-6, and 1-7.

(b) Low recovery may be due to a calibration error of the spectrophotometer.

Captions for Figures 12-17

Concentrations normalized with respect to percent dye recovered shown as a function of net effective fracture system volume (the product of production flow rate and residence time corrected for wellbore volumes) and normalized flow volume ($V/\langle V \rangle$) or residence time ($\theta = t/\tau$).

Figure 12

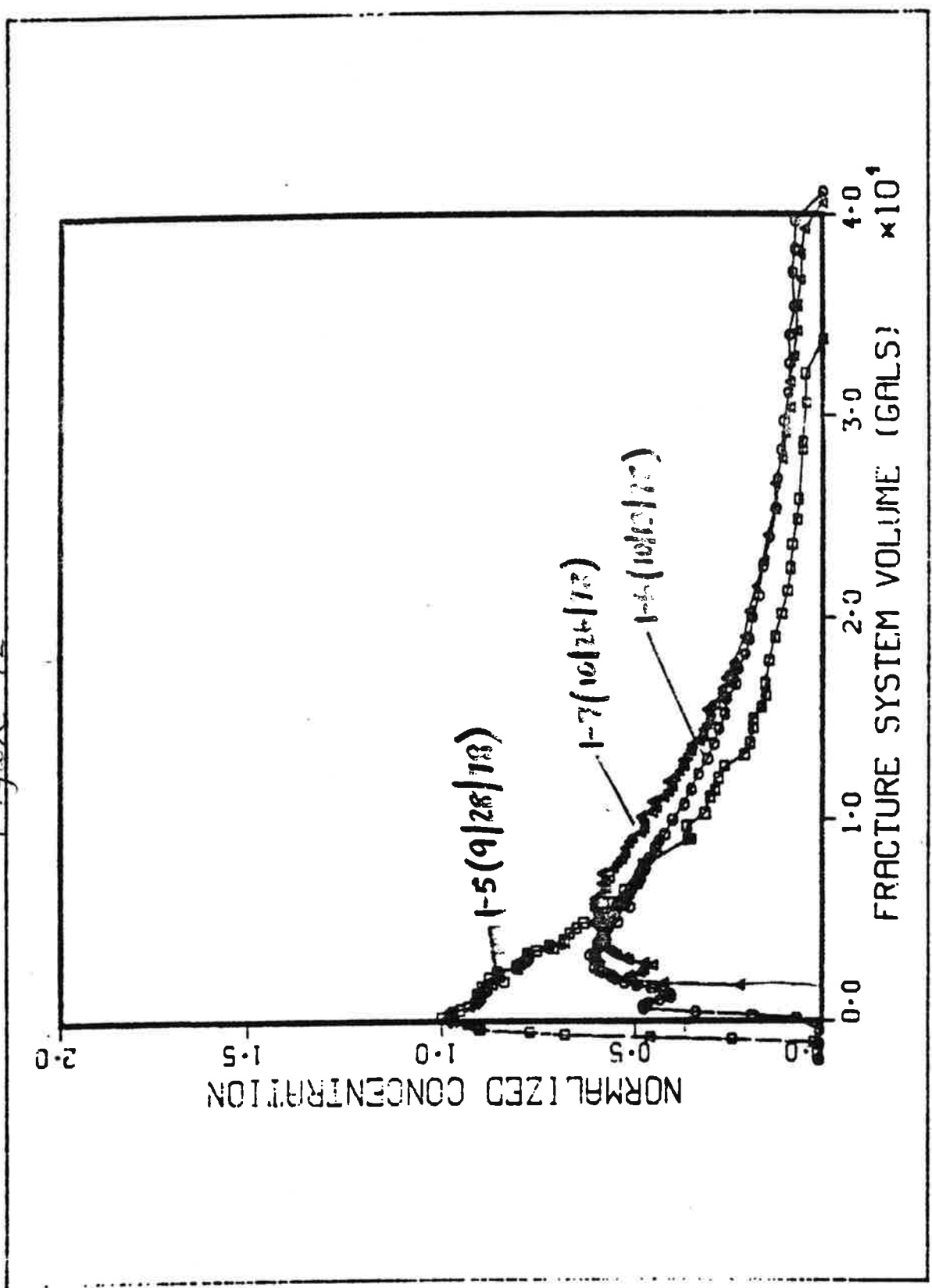


Figure 13

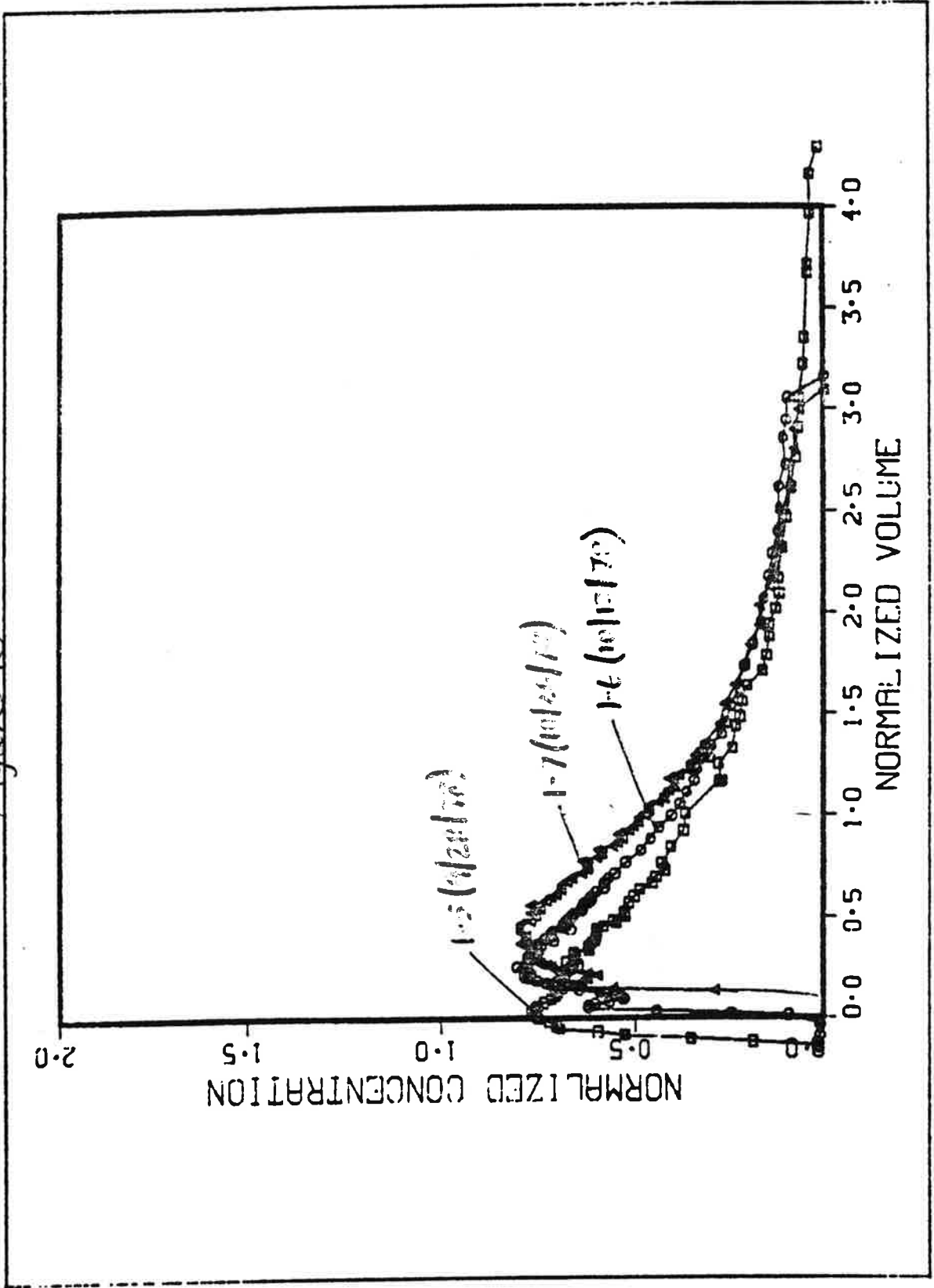


Figure 14

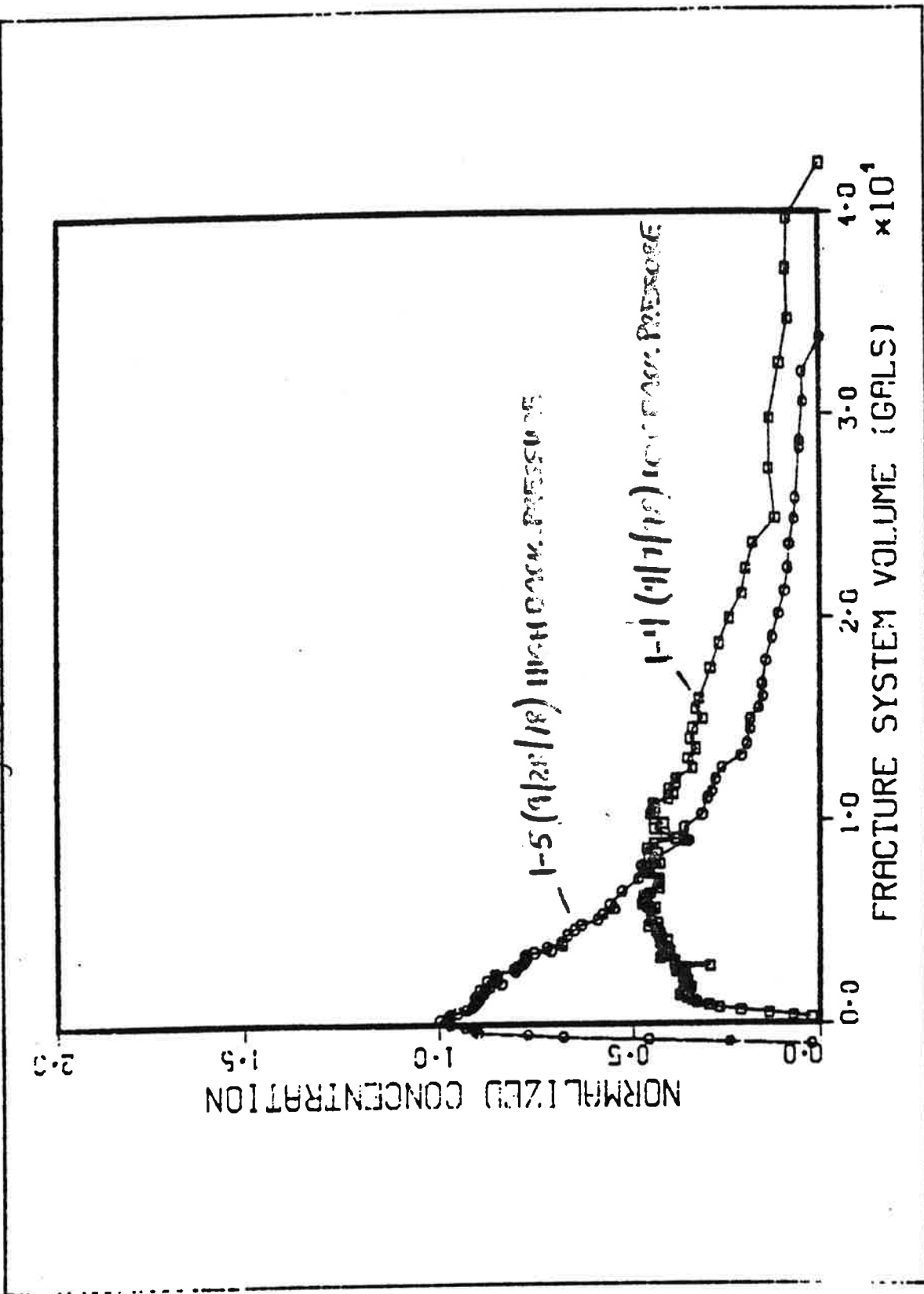


Figure 15

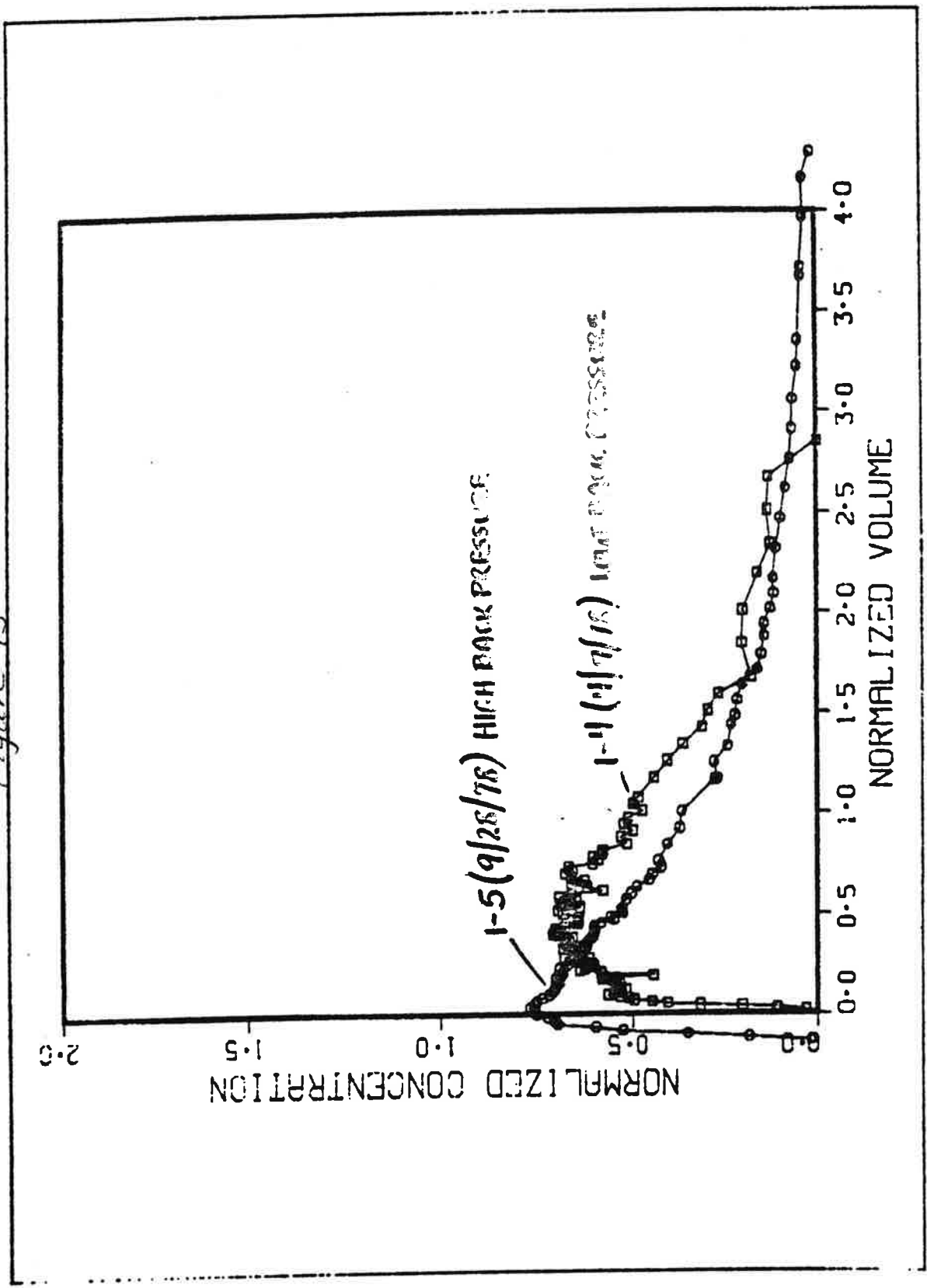


Figure 16

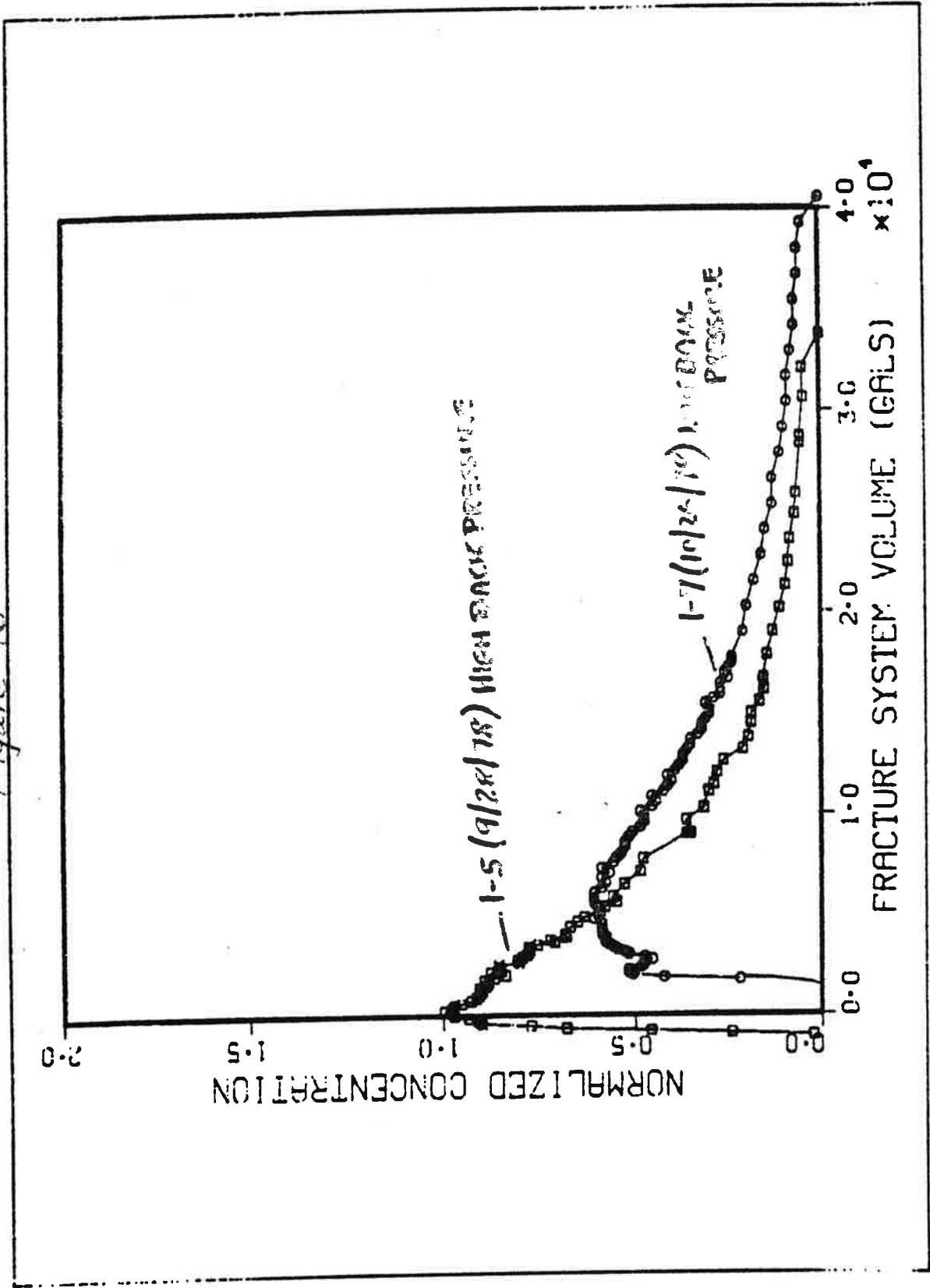
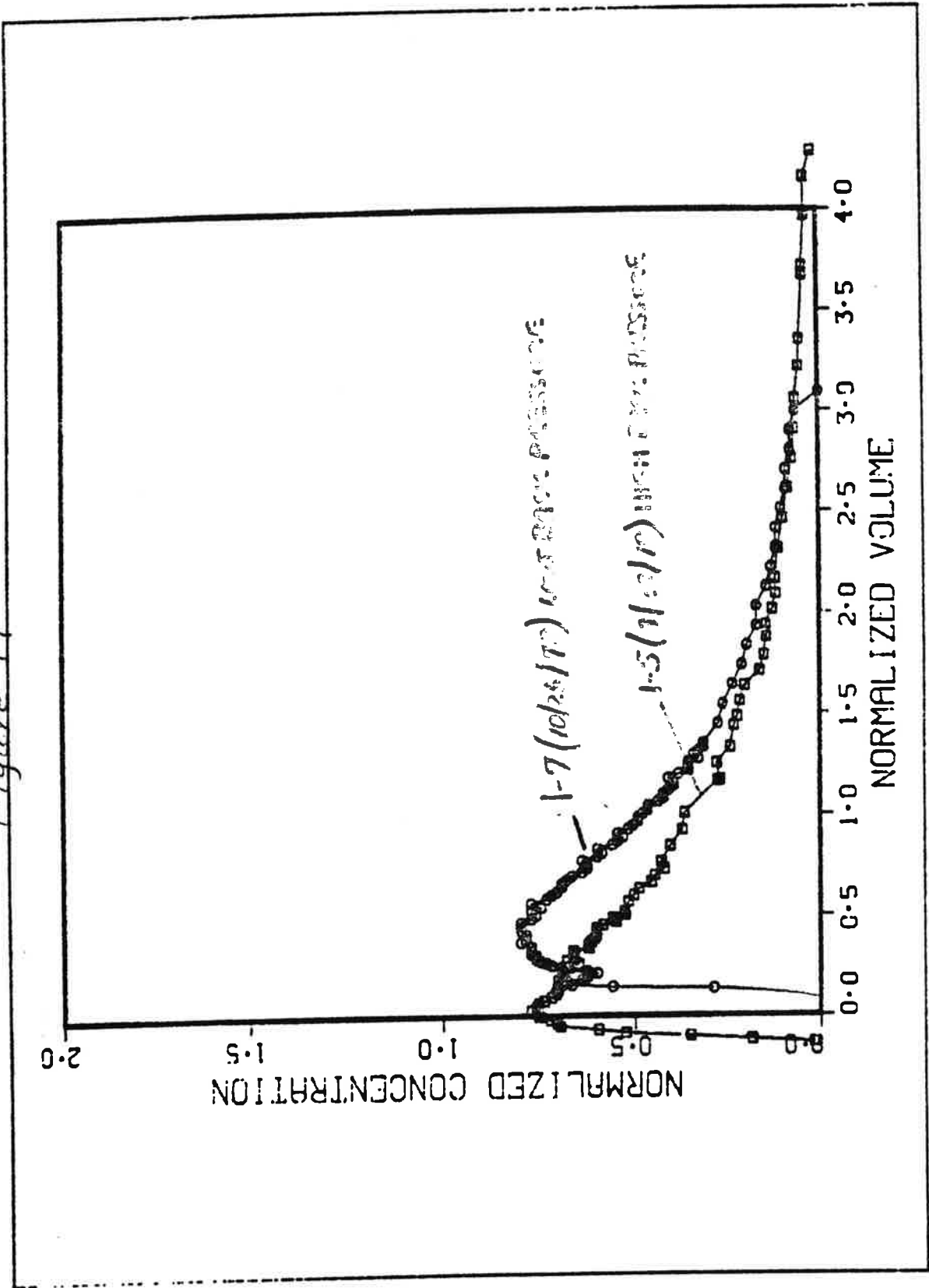


Figure 17



as determined by radioisotope injection logs, temperature surveys, and spinner surveys. There are two plausible explanations: First, a short-circuit path may exist behind the cement microannulus in EE-1 above 9000 ft, or a secondary injection zone may exist below 9050 ft with, in either case, a direct connection to a production zone high in GT-2B. Second, flow rates and resulting volumes from time integrations for GT-2B and EE-1 may be in error. A 10% error in either the EE-1 or GT-2 flowrate could explain the early arrival. The results of the second, high back-pressure experiment (1-6, 10/13/78) run at essentially the same conditions as the 1-5 experiment, suggest that flowrate errors may have caused the apparent early arrival and that the initial portion of both curves may overlap. A flowrate error of this magnitude has apparently not been observed in earlier dye tests.

In future experiments, inaccuracies of this character will be eliminated by using radioisotope tracers with logging in both injection and recovery wellbores.

- (2) If we assume that the 1-5 test had a flowrate measurement error, there are still differences between the high back-pressure experiments. For example, the difference in curve shape and peak concentration between the 1-5 and 1-6 tests is significant and may indicate that a change in flow pattern occurred between 9/28/78 and 10/13/78. (See Figs. 12 and 13.) The reduction of impedance over this period could be attributed to an increase in production rate in the deep zones of GT-2B (~8850 ft) which would lead to a somewhat

larger mean GT-2B wellbore volume (~ 1000 gal), but not enough to compensate for the observed differences in the tracer curves. A change in the flow pattern through that section of the fracture system which produces fluid at or near 8850 ft may be the cause of the observed differences.

- (3) The major portions of the high back-pressure residence time distributions (RTD) suggest that the fracture system volume is somewhat smaller and that the degree of mixing is different than under low back-pressure conditions (Figs. 14, 15, 16, and 17). Spinner surveys taken in the production zones of GT-2 during high and low back-pressure conditions (see Fig. 10) indicate a shift to a higher flow fraction in the lower section (~ 8850 ft) of GT-2B, 69% with 1400 psi back pressure and $\sim 20\%$ with 200-250 psi back pressure. This effect could certainly lead to a different RTD as well as a mean fracture system volume.
- (4) The general shape of all RTD curves is consistent with a model where the observed large dispersion effect is caused by a superposition of mixed flows in the GT-2B wellbore each having a much smaller degree of dispersion. Furthermore, the Na-fluorescein tracer tests have revealed, at the very least, that distinct qualitative flow pattern differences exist between high and low back-pressure conditions.
- (5) Dye was observed in the EE-1 annulus on all three experiments (1-5, 1-6 and 107). A preliminary analysis of the data indicated that approximately 25-40 gal/min flowing in the open annulus above the cement in EE-1 could account for the observed dye. Later

experiments with Br^{82} have verified that flow is occurring in the cement microannulus and above the cement in EE-1 at approximately these flow rates.

VI . PERMEATION FLOW ANALYSES

The data from Expts. 185 and 186 have been analyzed in terms of the diffusion mode (3,9, and 10). The data and theoretical fits are presented in sections A, B, C, and D. During Expt. 185, two separate pressurizations of EE-1 with GT-2 shut-in provided data on flow into permeation. Expt. 186, the high back-pressure experiment, provided data on both the early- and long-term water losses with both EE-1 and GT-2 pressurized to near S_3 .

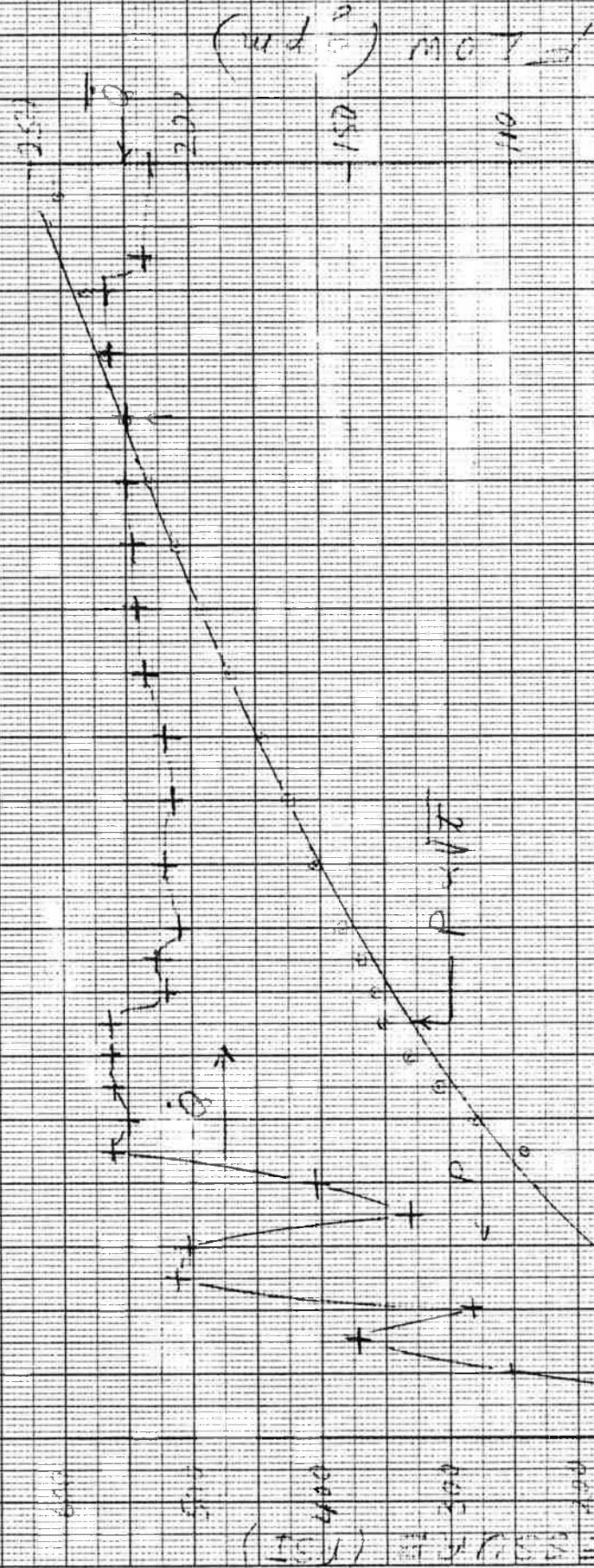
A. Early-Time Low-Pressure Data

Figures 18, 19, and 20 are plots of the EE-1 flow (indicated by \dot{Q} and +) and pressure (P and .) for the first 30 minutes of the two pump ups of Expts. 185 and 186. Buoyancy has little effect at early times and the data has not been corrected. In each case the pressure data has been fit to a $P \propto \sqrt{\text{time}}$ curve (solid line). From these curves the value of $A\sqrt{kB/B_R}$ was calculated and is annotated on each graph. The flow was assumed to be a step function starting at t_0 and having the value \dot{Q} as indicated on each graph. These values are approximately twice those measured on previous experiments with GT-2 vented.

B. Early-Time High-Pressure Data

After the pressure becomes greater than ~ 4.0 MPa (600 psi), the constant flow case pressure departs from the square root of time behavior. Figures 21, 22, and 23 indicate the quality of the data in the high pressure

FIG. 18 XP 180T: FLOW PRESSURE AND HEAD AT PUMP UP



$$\text{AVG. FLOW} = 3.84 \text{ cm}^3$$

57.50
1/1/11

57.50

57.50

THE 19 AMP INTAKE PUMP HEADLINE AND FLOW 2nd PUMP UP

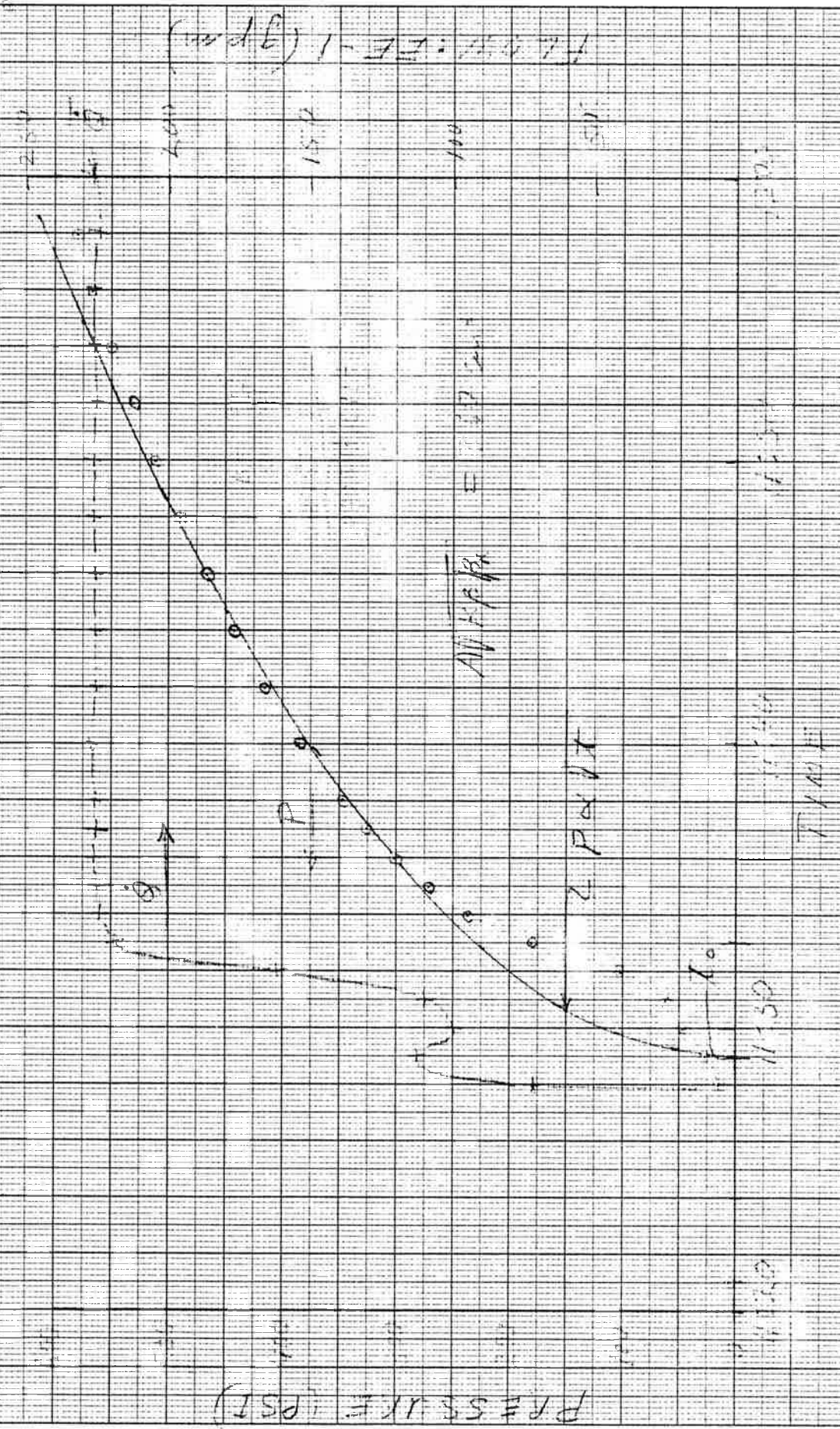


FIG. 20 EXP 186: EF-1 PRIMER WITH AIR 1 LPM

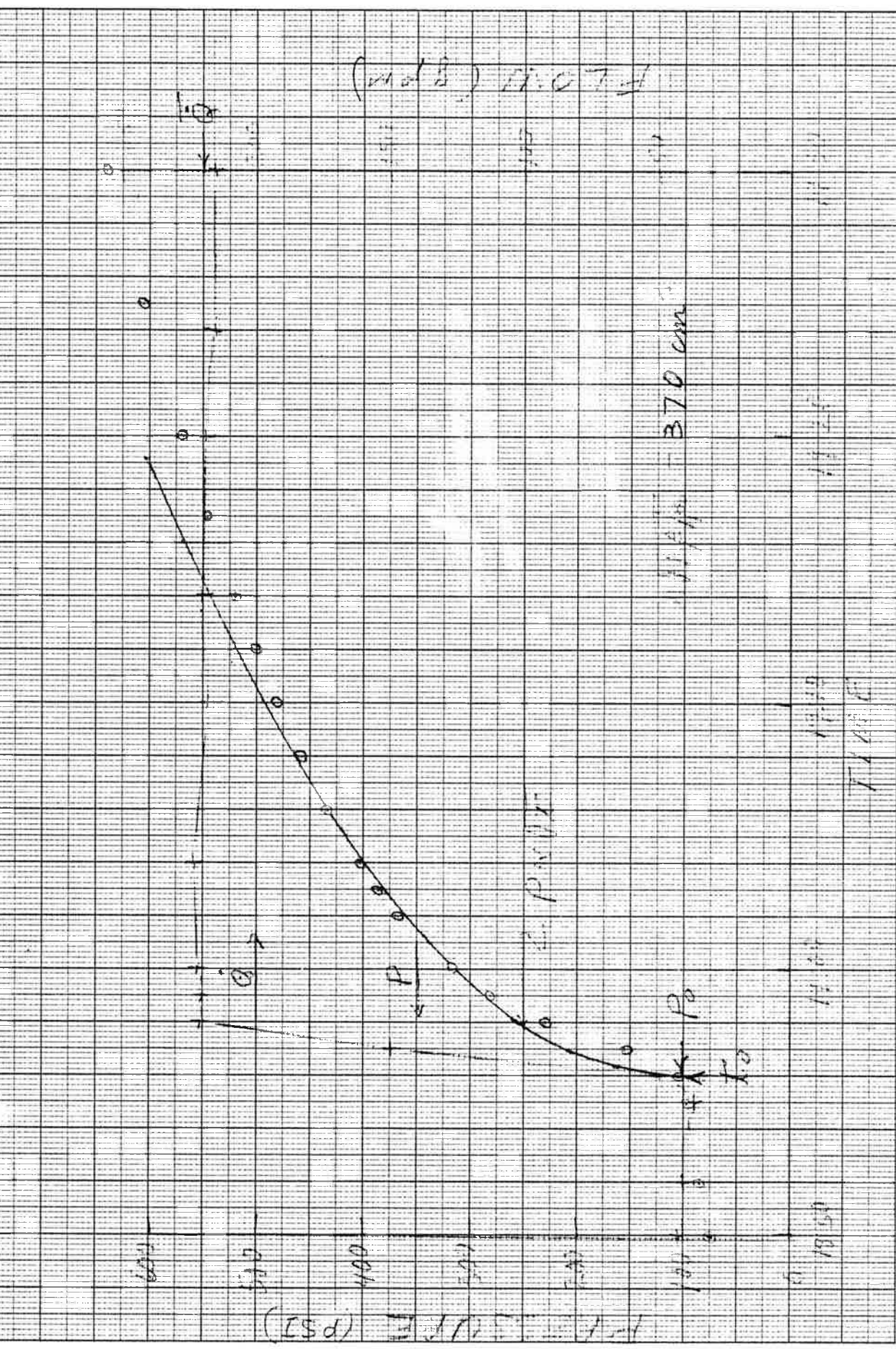


FIG. 21 EXPERIMENT: PRESSURE AND FLOW IN PIPELINE

250

GT-R

$\dot{Q}(EFF)$

200

PRESSURE (PSI)

150

$P(EFF)$

$P(GT-R)$

100

50

500

500

TANK (HP)

87.2

1 1/2 2 3 4 5 6 7 8 9 10

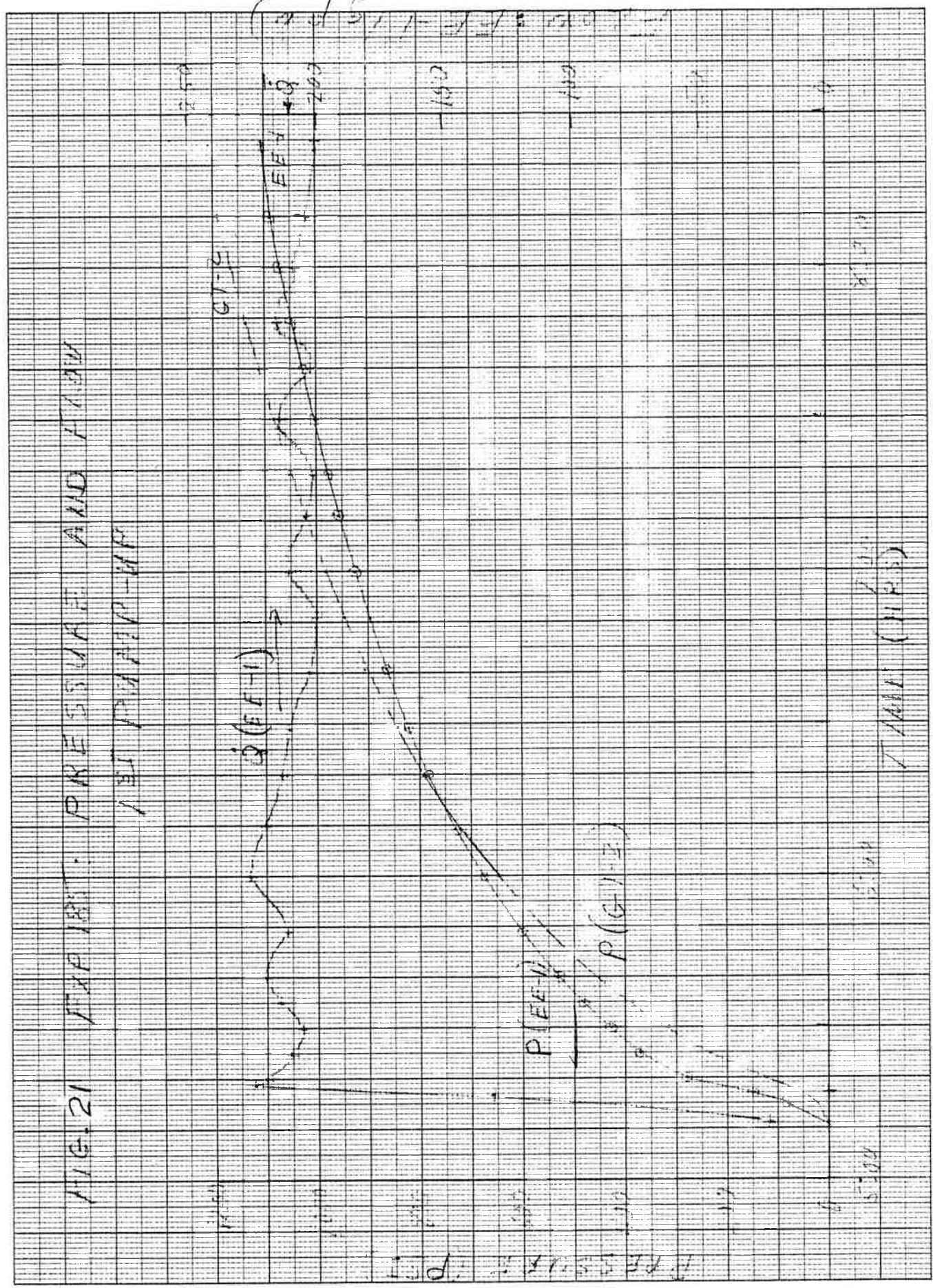
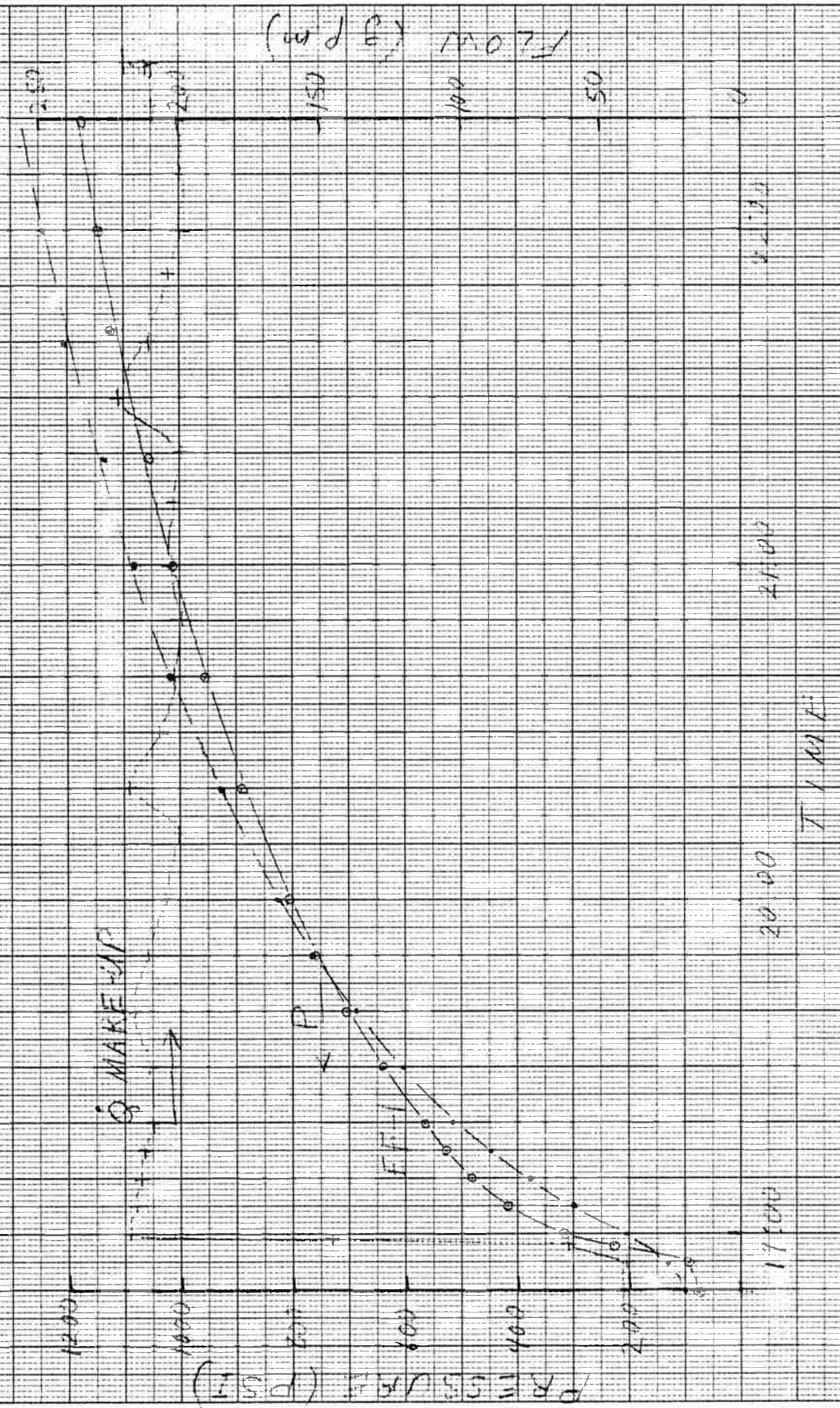


FIG. 23 EXP 186: PRESSURE AND FLOW



range for the three pump-ups. Each is a plot of the permeation flow (either EE-1 or EE-1 minus GT-2) and the wellhead pressures for EE-1 and GT-2. The permeation flow is approximately the same in each case and is constant to within 10% over the range of interest. An examination of the EE-1 and GT-2 pressure plots indicates the results are the same for all three pressurizations.

The second pressurization of experiment 185 had the longest period of constant flow (over 4-5 hours) and an initial reservoir pressure of zero. Since the period of constant flow is longest and the pressure reached at constant flow is highest, this is the best of the three for comparison with the pressure-dependent diffusion model^(3,9). Figure 24 is a plot of the EE-1 pressure increase corrected for buoyancy. The solid line fit to the data is the results of any AYER calculation of the pressure-dependent model with constant flow over a circular fracture.

C. Long-Term Water Loss

After 16 hours of pumping the EE-1 surface pressure reached 1330 psi and was stabilized within a few percent of this value. The flow into permeation during this constant pressure phase is plotted in Fig. 25. The data has been corrected for the controlled leak at the GT-2 packoff. The solid line fit to the data is again the result of an AYER calculation of the pressure dependent diffusion model with a constant fracture pressure. The long-term diffusion flow, while masked by the developing leak up the EE-1 annulus, after the eighth day of Expt. 186, still appears to be approximately twice that measured during the 75-day Phase I test.

FIG. 24

EXPERIMENTAL EFFICIENCY
2nd PUMP-UP

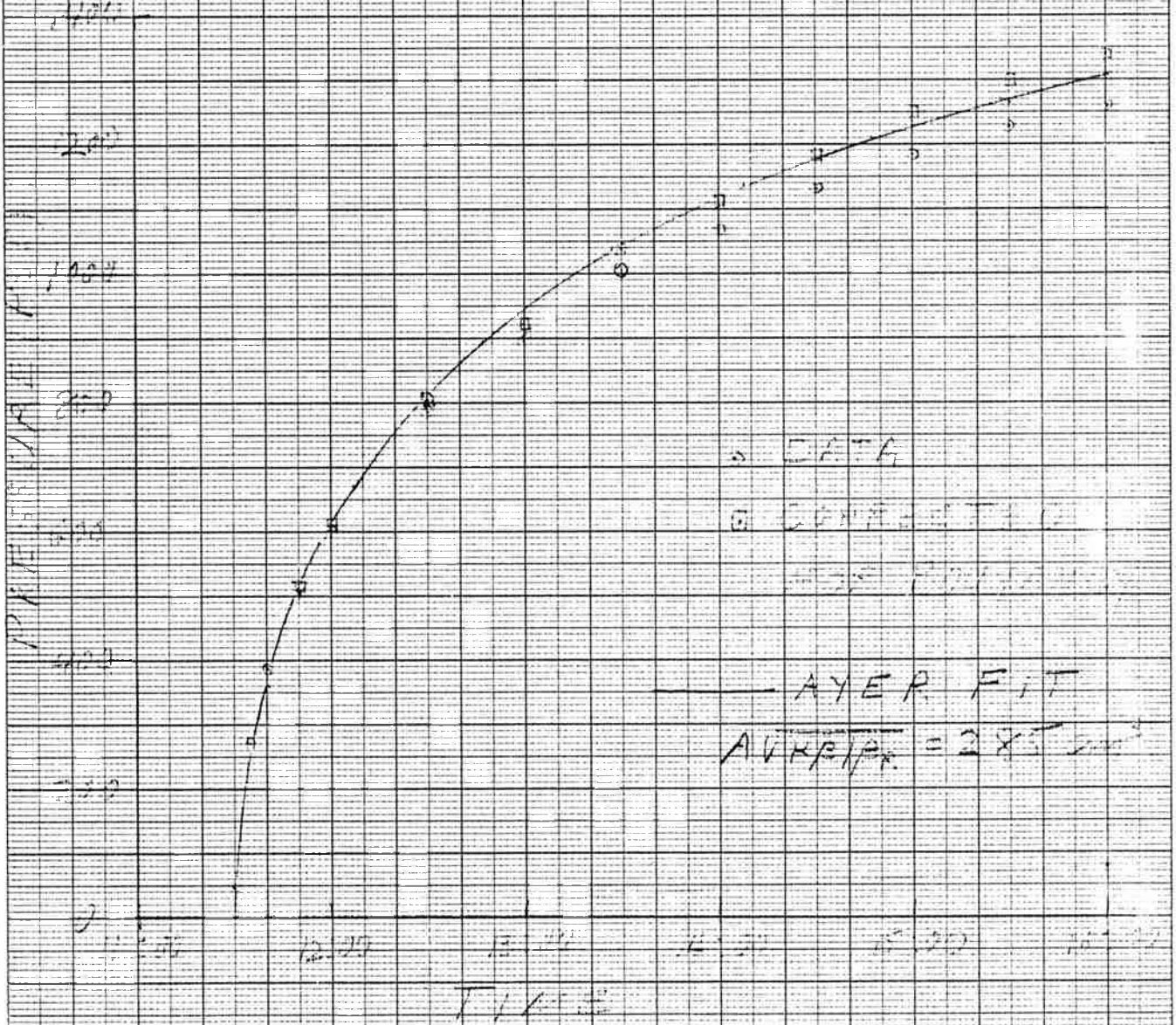
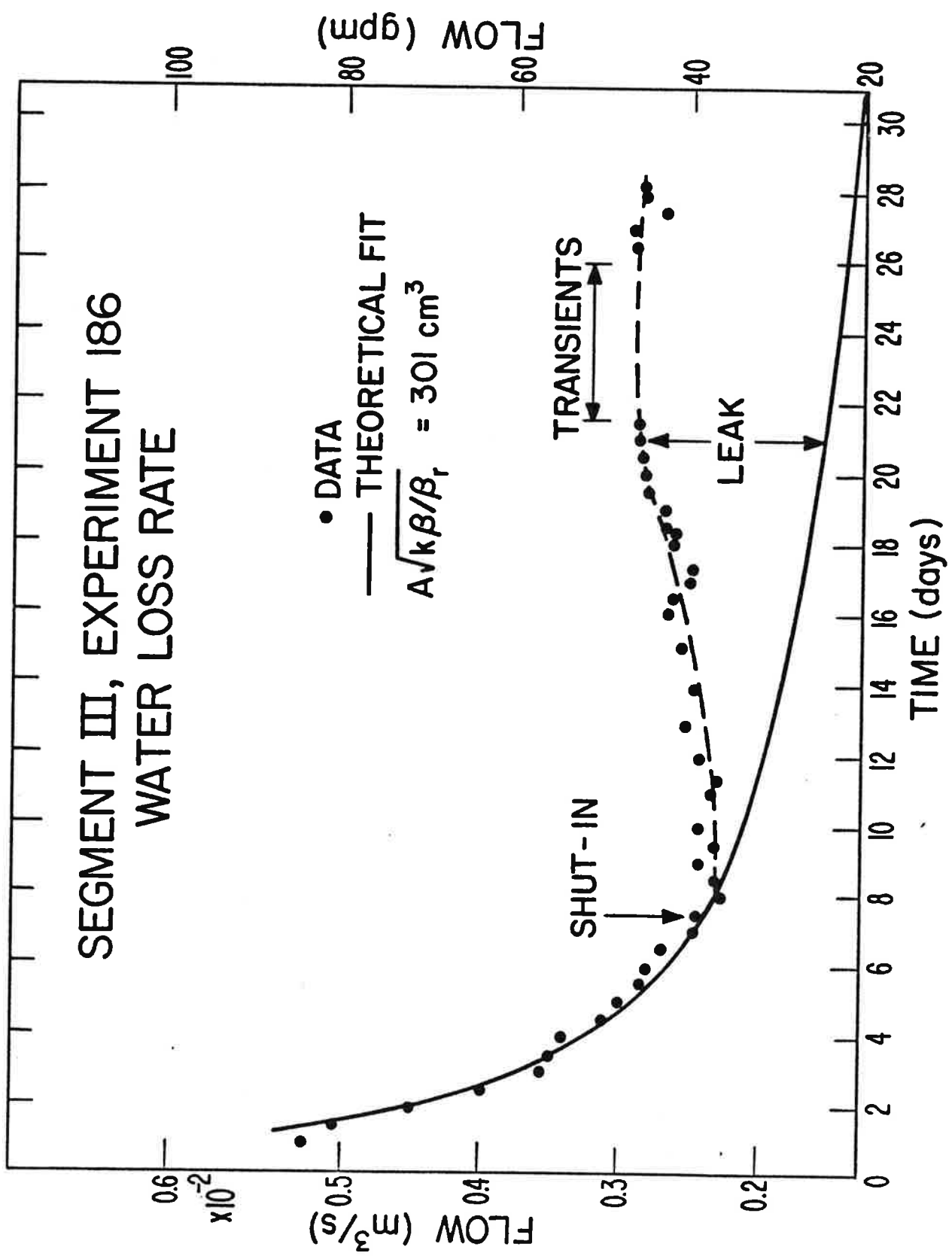


Figure 25



During the seventh day of operation (Sept. 25) both wellbores were shut-in to measure the buoyancy. After this operation the water losses no longer match the expected theoretical rates but increased gradually to about $0.32 \times 10^{-2} \text{ m}^3/\text{s}$ (51 gpm) at the conclusion of Expt. 186 on Oct. 16. The difference between the theoretical curve and the data is replotted in Fig. 26. The rate of increase of this leak with time is seen to be nearly constant at approximately 1.0 gpm/day. The total amount of water lost to this leak was 1660 m^3 (438,000 gallons).

However, the inferred 25 gpm flow bypass up the EE-1 annulus at the end of Expt. 186, as shown in Fig. 26, is considerably less than the 40 gpm leak rate measured following this experiment (4). The balance of this measured flow bypass up the EE-1 annulus may well have existed throughout Expt. 186. If this additional leak up the EE-1 annulus were to have been constant at about 12 gpm throughout Expt. 186, then the fluid loss rate under high back-pressure may actually have been similar to that measured during the 75-day low back-pressure flow test, as shown in Fig. 27.

If the fracture itself was similarly pressurized under either low* or high back-pressure flow conditions, one would not anticipate that the fracture system water loss rates would be appreciably different between these two long-term flow tests.

D. Summary

With both EE-1 and GT-2B pressurized to a level approaching S_3 , the characteristics of the system are generally those for the combined system. The diffusion parameter and long-term water losses reflect the properties of the fracture systems connected to both wellbores. The permeation

*As shown in Section III above, under low back-pressure flow conditions, the majority of the fracture system pressure drop occurs at or near the fracture exit.

Figure 27

PHASE I WATER LOSS DATA

--- THEORETICAL

○ FIT

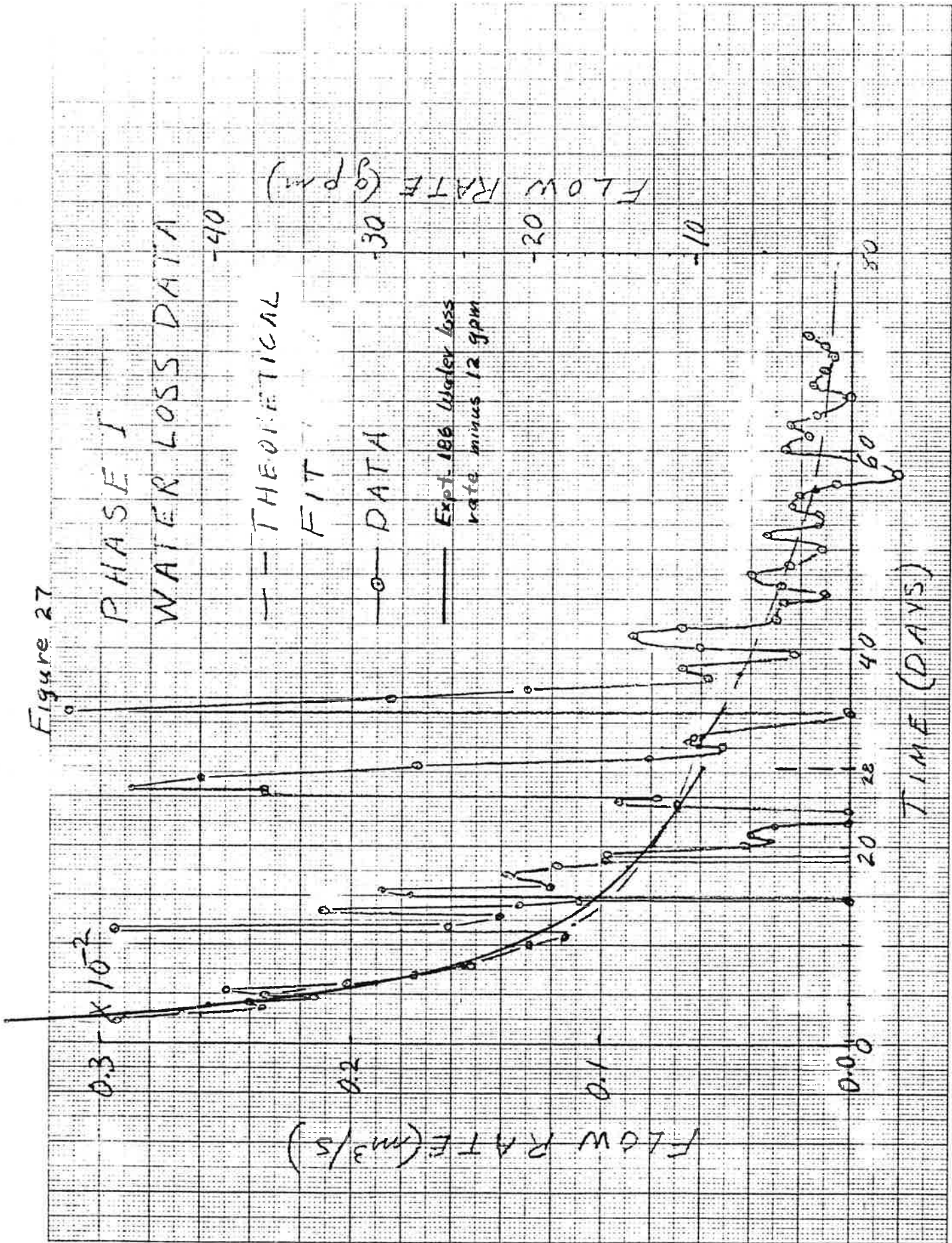
— DATA

— Expt. 186 Water loss
rate minus 12 gpm

FLOW RATE (gpm)

FLOW RATE (m³/s)

TIME (DAYS)



flow in all phases of the experiments was approximately twice that measured in Segment II with only EE-1 pressurized. However, the long term water loss rates may actually have been comparable. The resulting values of the diffusion parameter $\alpha = A\sqrt{k\beta/\beta_R}$ at hydrostatic pressure are summarized in Table VI. A similar discrepancy between the short- and long-term values of α was noted in the Phase I data. This discrepancy is probably due to the heterogeneity of the reservoir; in particular the low impedance connection between the fracture systems. The pressure dependence of α remains the same as in past experiments.

TABLE VI

Exp.	$A\sqrt{k\beta/\beta_R} (m^3)$	
	185	186
Short Term	$0.372^* \times 10^{-3}$	0.373×10^{-3}
Long Term	0.285×10^{-3}	$0.301^{**} \times 10^{-3}$

*Average of two measurements.

**Constant pressure, others are constant flow.

Diffusion parameter measured in experiments 185 and 186.

VII. FLUID CHEMISTRY DATA

During Expt. 186, one sample per day was collected at each of the following points:

1. GT-2 filtered through a .45 μ millipore filter
2. GT-2 not filtered
3. EE-1 not filtered
4. Make-up water - filtered through 100 μ filter.

These samples were analyzed for pH, conductivity, bicarbonate, chloride, fluoride, sulfate, sodium, potassium, calcium, magnesium, iron, lithium and silica by techniques described in the Phase I, Segment 2 report.⁽³⁾

A. Results

The results of the analyses are presented in Figs. 28-37. Unlike the results of the Phase I, Segment 2 run, the species in this experiment did not build up to some steady level but rather showed some decline in concentration (see Figs. 28 and 29). The main reason for this decline was the extremely high makeup flow rate (often as high as 30% of the total flow rate) due to high water losses in the formation and to leaks in the system. This high makeup flow completely dominated the mixing and therefore the buildup of dissolved species with time. The slight decline observed in several of the graphs could be due to the addition of "dirty" GT-2 water to the EE-1 pond early in the experiment. This "dirty" water was needed because the high water losses drained the pond much faster than the 400-foot well could supply. After the water from the GT-2 pond was added, water from San Antonio Creek was hauled up to supplement the supply well. The addition of "clean" makeup water would dilute the earlier "dirty" water causing the decline. An analysis of the GT-2 pond "dirty" water is included as Table VII. Also included is a Table VIII of trace element concentrations courtesy of I. Binder of CNC-11.

B. Preliminary Interpretations

The graph of SiO_2 vs time (Fig. 37) is the basis for the following tenuous interpretation. The SiO_2 vs time curve has a steady slope of -1.1×10^{-4} ppm/min. This change in concentration can be evaluated using the reservoir

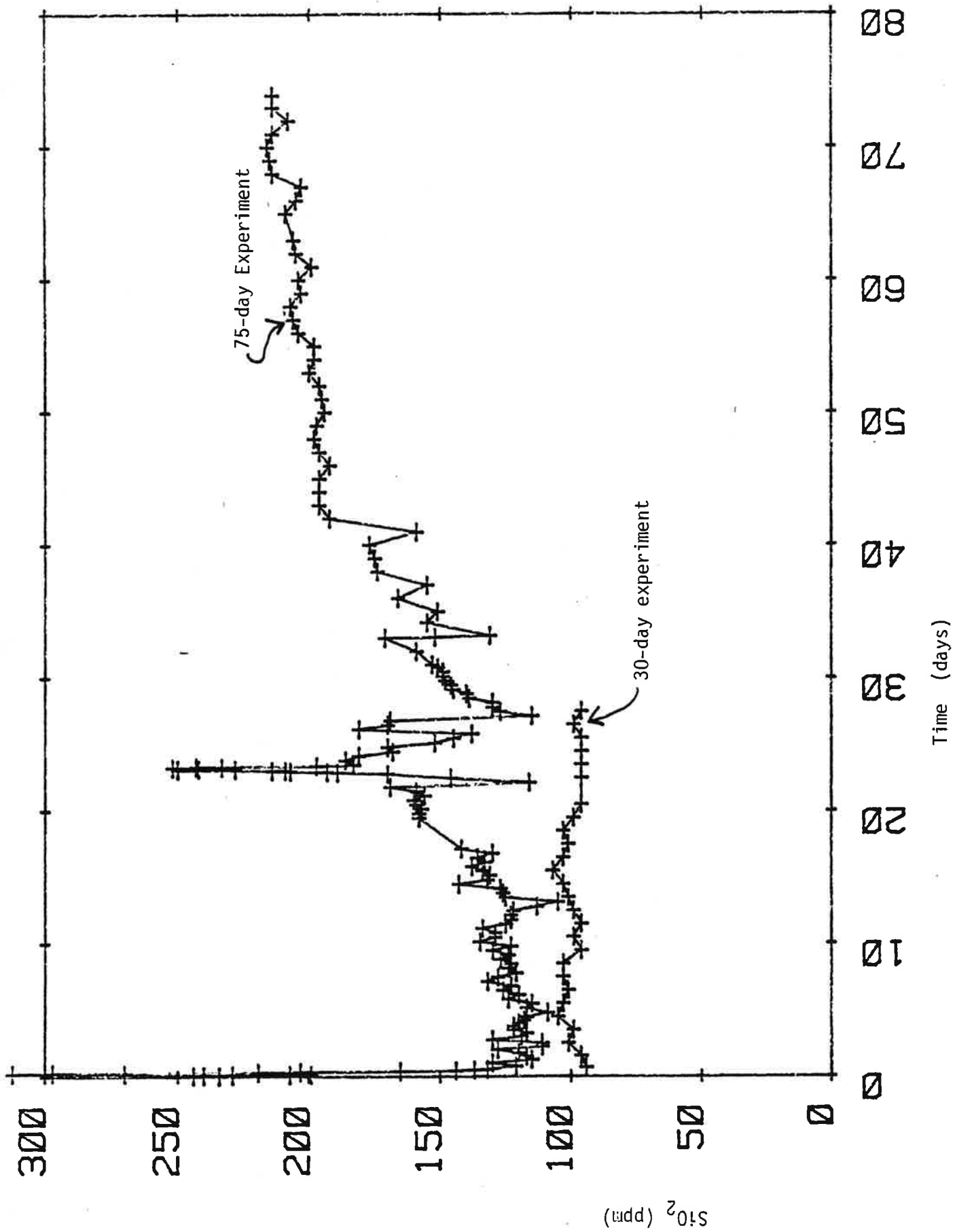


Fig. 28. Silica vs time for the 75-day Experiment and the 30-day experiment.

Fig. 29. Conductivity vs time for 75-day Experiment and 30-day Experiment.

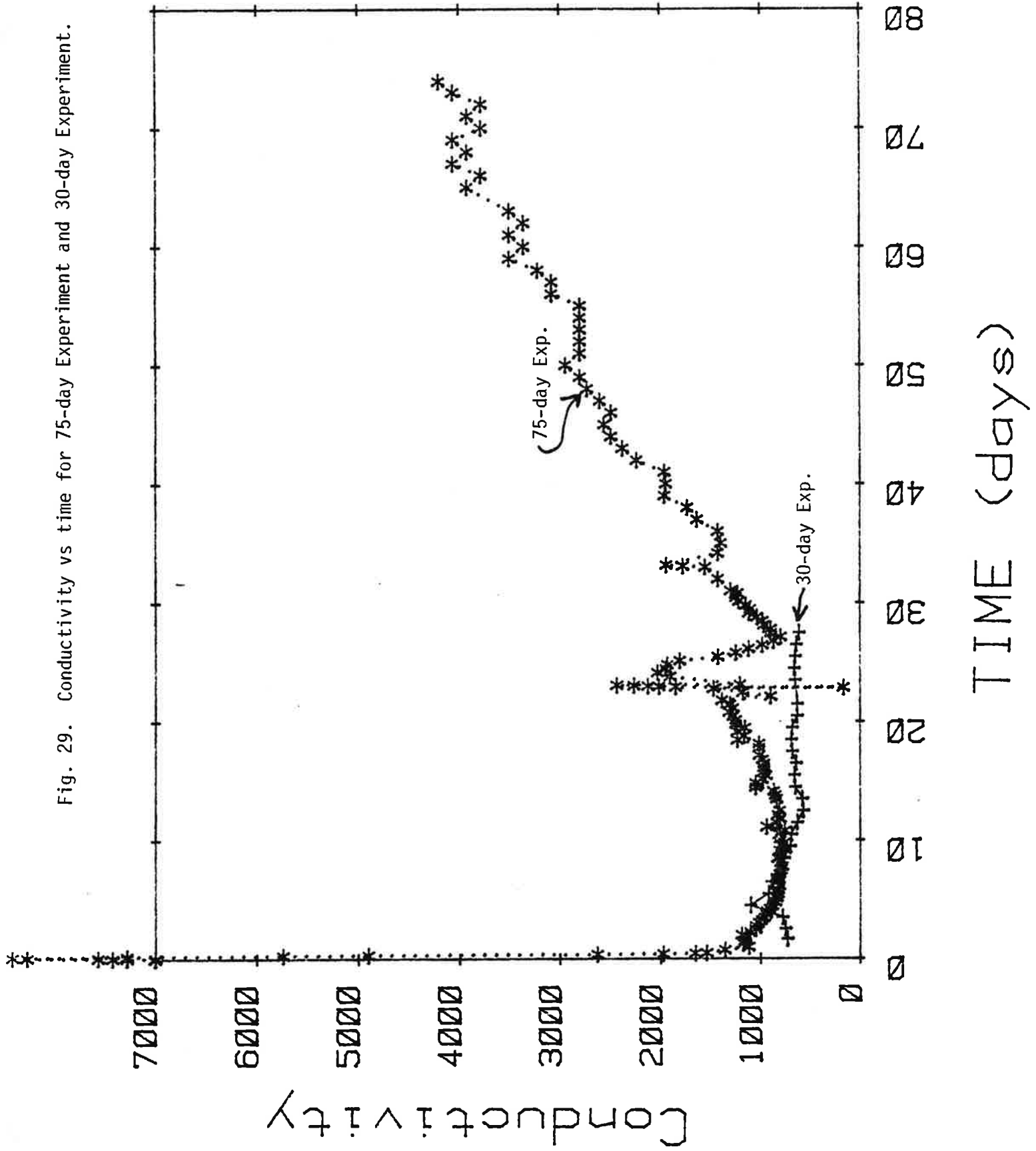


Fig. 30. Conductivity vs time.

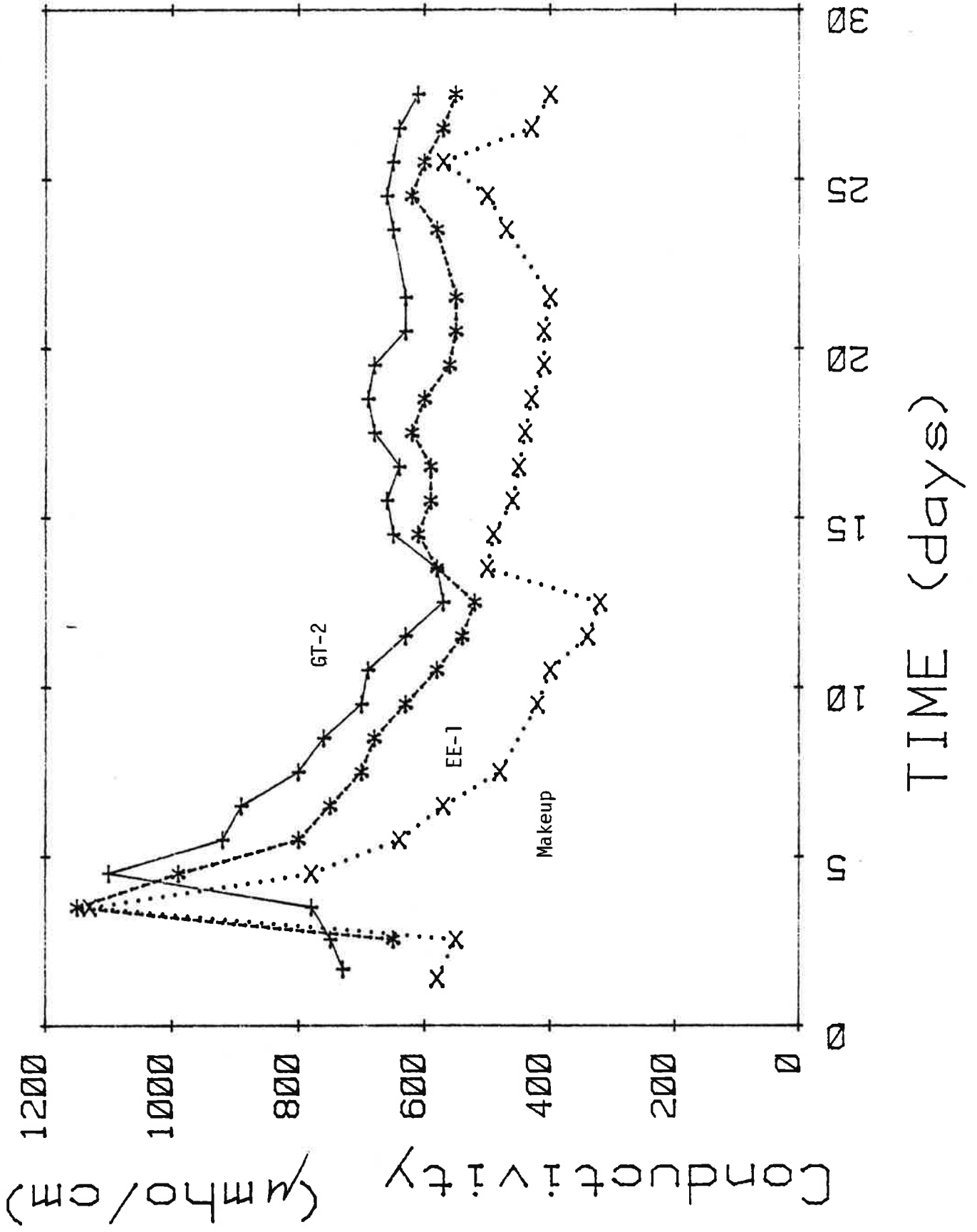


Fig. 31. pH vs time.

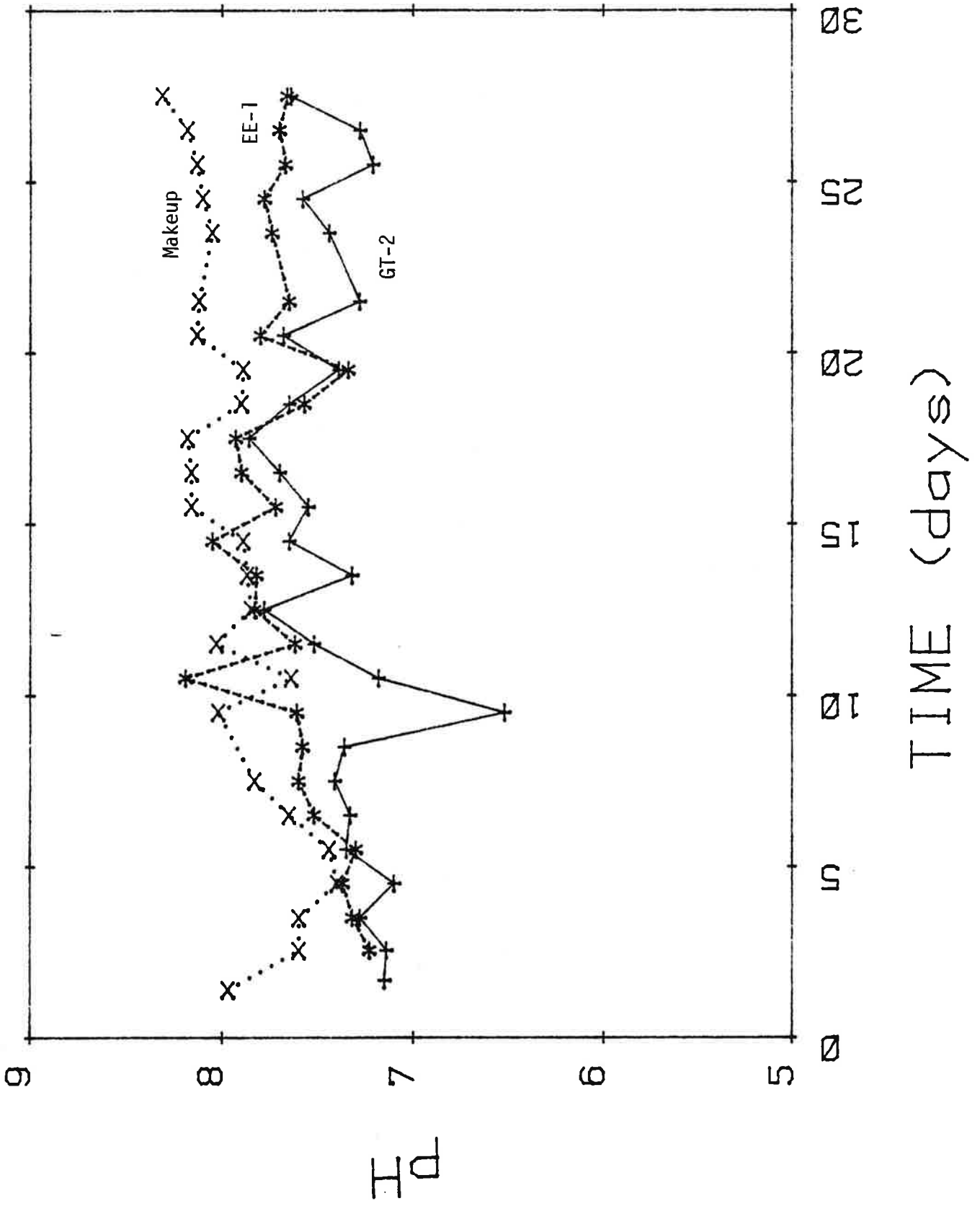


Fig. 32. Chloride vs time.

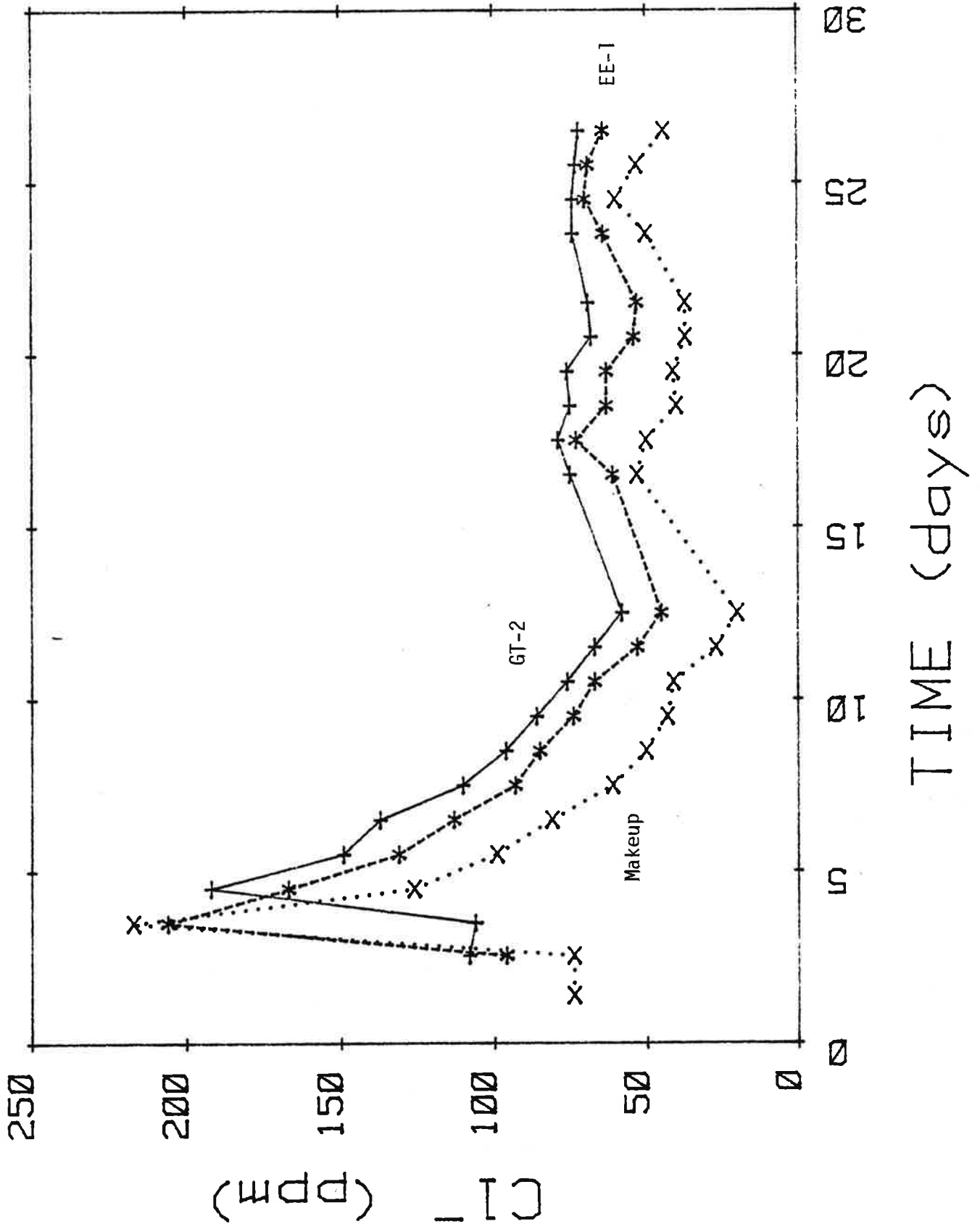


Fig. 33. Bicarbonate vs time.

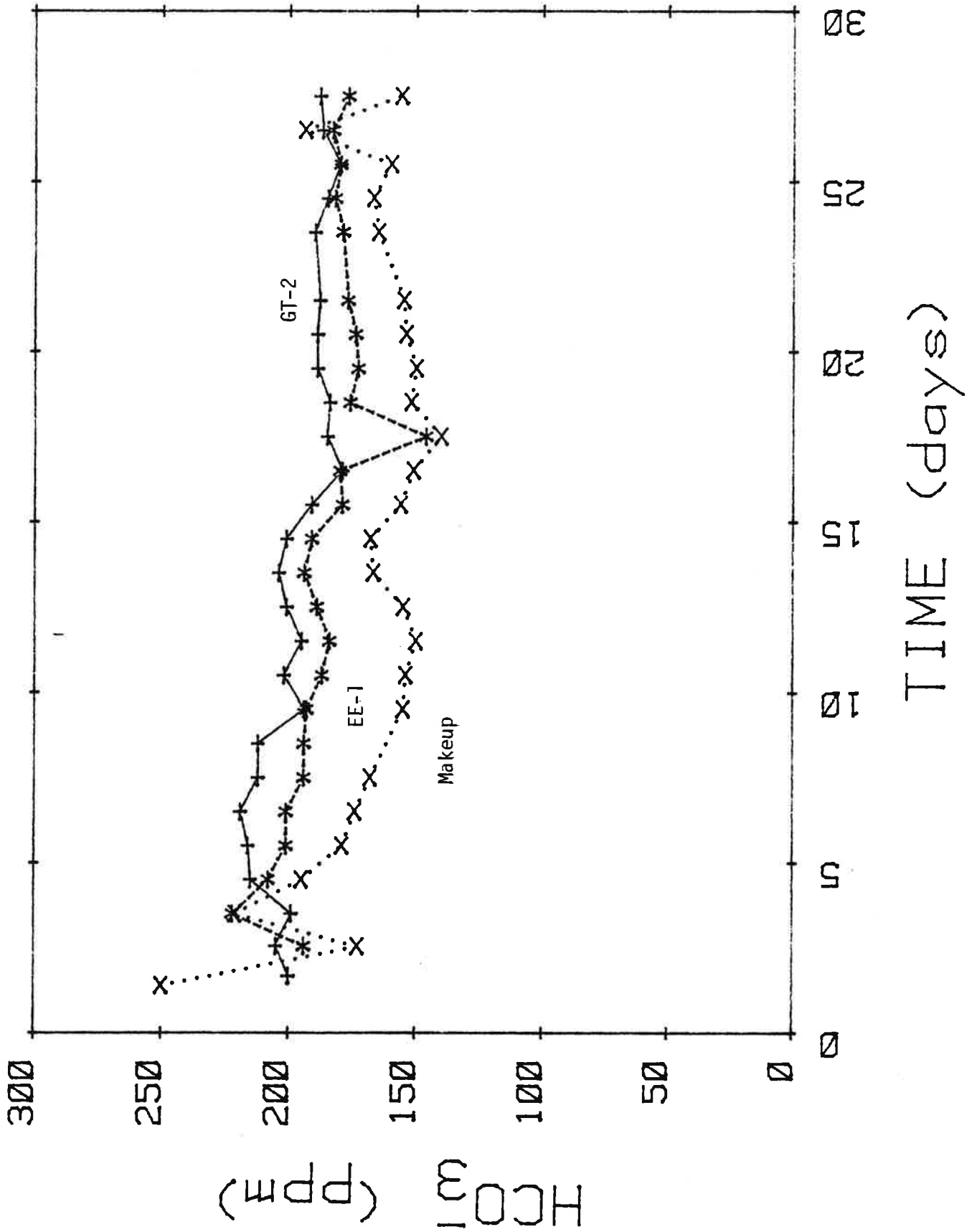
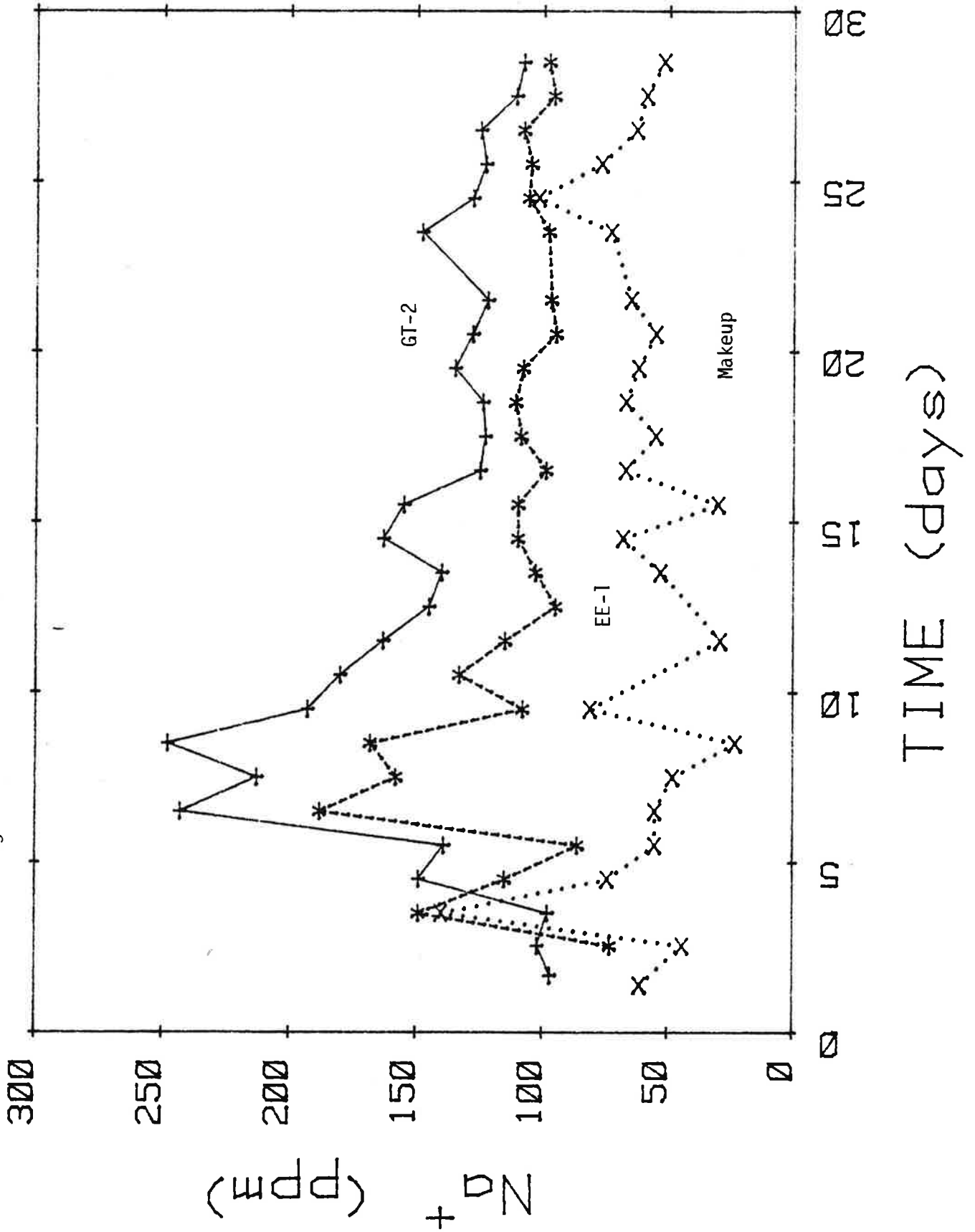


Fig. 34. Sodium vs time.



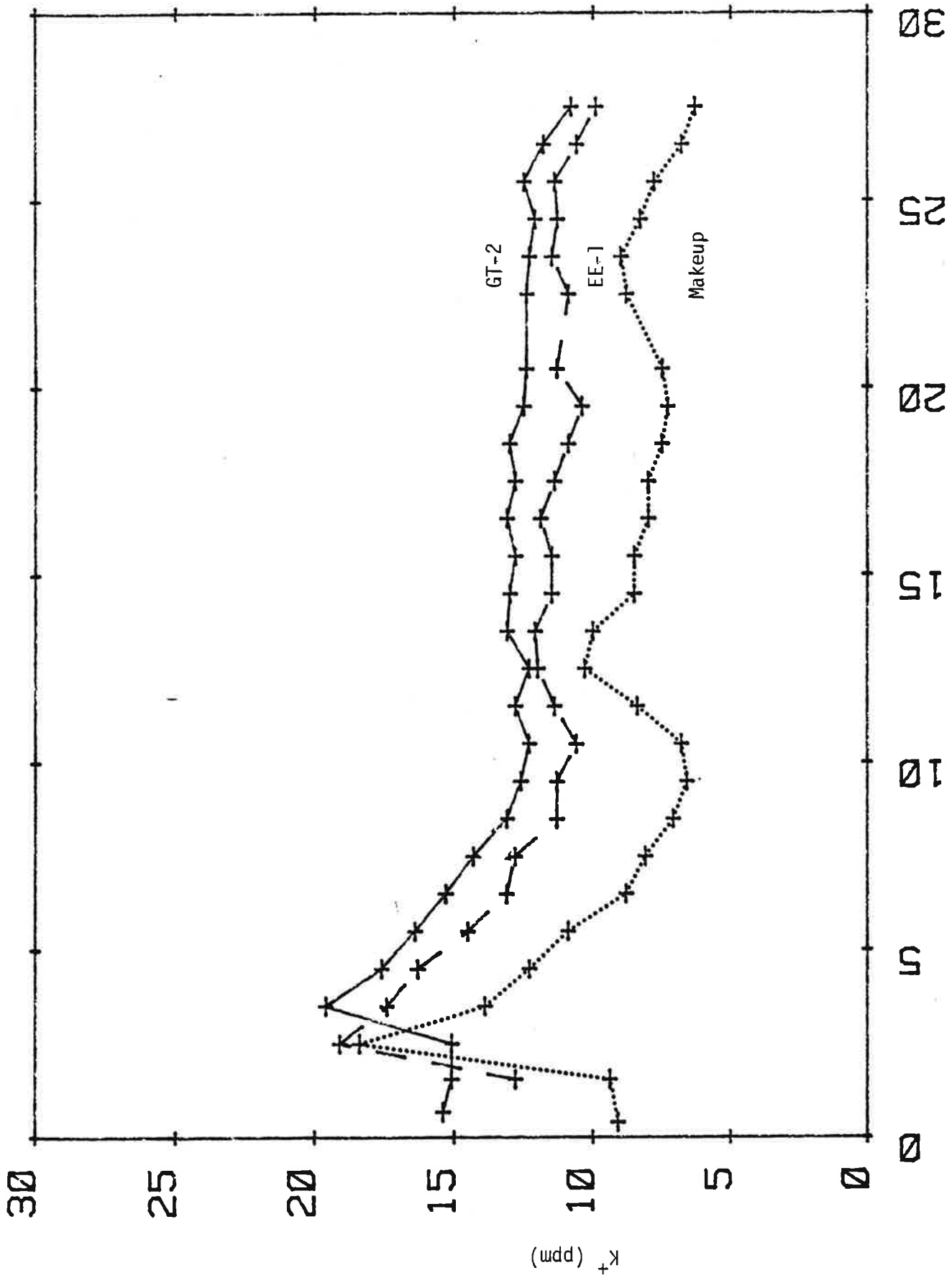
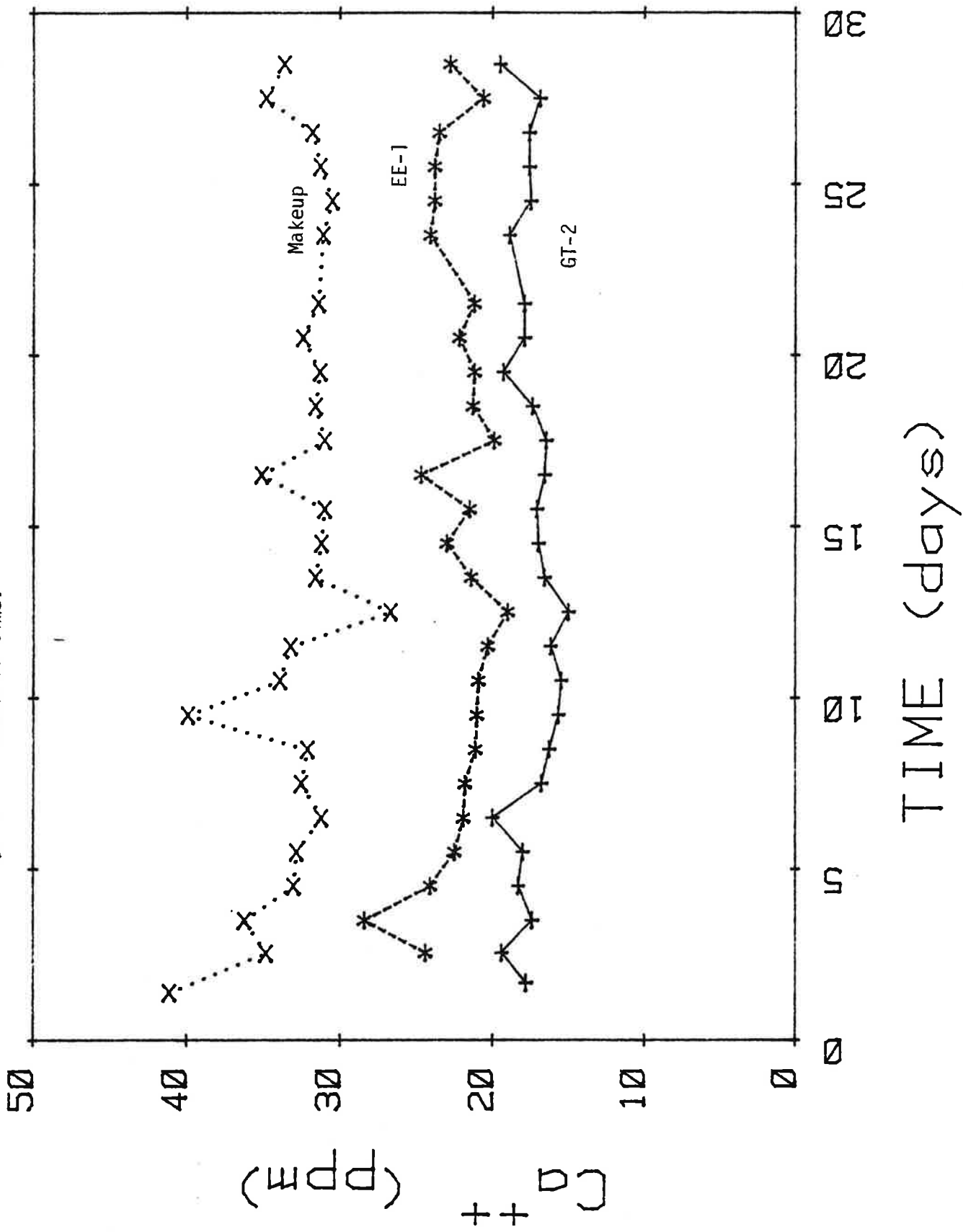


Fig. 35. Potassium vs time.

Fig. 36. Calcium vs time.



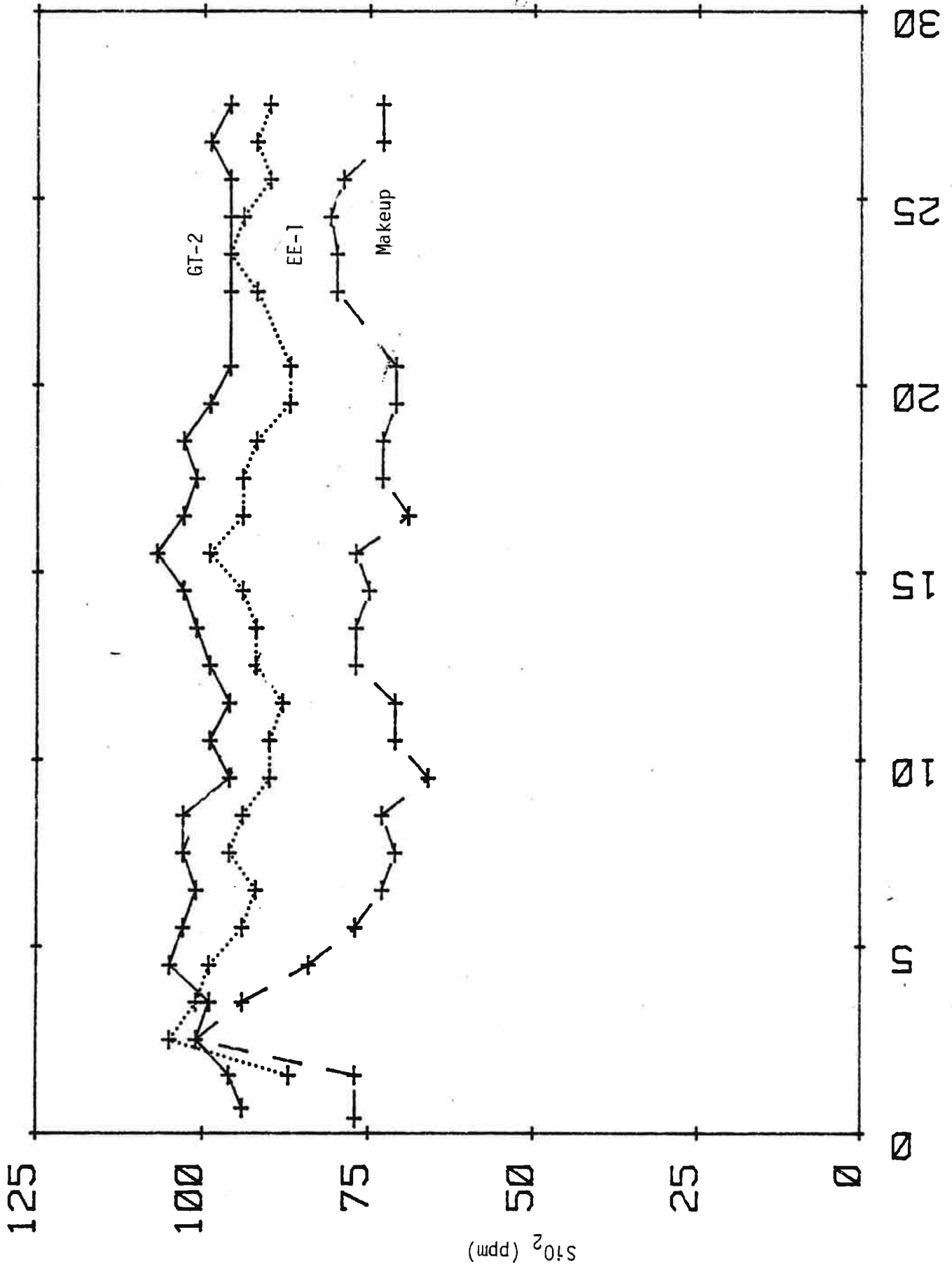


Fig. 37. Silica vs time.

TABLE VII

ANALYSIS OF GT-2 POND WATER - September 20, 1978

SiO ₂	181.4 ppm
Na	580 ppm
Ca	49.4 ppm
K	318 ppm
Mg	2.6 ppm
Fe	4.4 ppm
HCO ₃ ⁻	362.8 ppm
Cl ⁻	1102 ppm
F ⁻	4.2 ppm
pH	7.74
Conductivity	3600 μs/cm

Σ cations = 36.22

Σ anions = 36.99

TABLE VIII

Concentration of Elements in Expt 186 Water ($\mu\text{g/g}$)

Sample	3GF	7GU	7GF	9 _a GF	14GF	17GU	17GF	26GF	28GU	28GF
Date	1210 19 Sept 78	1210 22 Sept 78		1200 24 Sept 78	1200 29 Sept 78	1200 2 Oct 78		1200 12 Oct 78	1200 14 Oct 78	
Day	0	3	3	5	10	13	13	23	25	25
Na	113	145	149	243	163	150	163	128	125	125
K			13.0		13.5	10.3	16.1	19.3	16.9	13.1
Ca	8.46	12.3	11.7	19.8	20.4	22.1	23.3	19.7	20.1	18.3
Sc						2.75×10^{-6}			5.6×10^{-6}	
Fe	.215	.0321	.0561	.865	.722	.134	.0963	.0747	.0511	.548
Co	6.8×10^{-4}	2.0×10^{-4}		2.5×10^{-4}	1.4×10^{-4}	1.45×10^{-4}	1.65×10^{-4}	3.65×10^{-4}	1.3×10^{-4}	8.7×10^{-5}
Zn	.0154	.0161				.0148		.00303		
As	.153	.0967	.0955	.176	.133	.109	.117	.111	.104	.0971
Br	.503	.953	.980	1.02	.682	.655	.743	.600	.568	.558
Sr	.188	.342	.246	.531	.343	.304	.324	.305	.272	.241
Sb	7.7×10^{-4}	9.0×10^{-4}	8.7×10^{-4}	1.6×10^{-3}	1.6×10^{-3}	1.9×10^{-3}	2.0×10^{-3}	2.15×10^{-3}	1.8×10^{-3}	1.3×10^{-3}
Cs	.264	.223	.204	.366	.275	.231	.261	.205	.198	.192
Eu	2.0×10^{-5}	1.4×10^{-5}		2.6×10^{-5}	1.5×10^{-5}	1.3×10^{-5}	1.8×10^{-5}	1.5×10^{-5}	1.7×10^{-5}	1.6×10^{-5}
W	.0213	.0235	.0200	.0416	.0311	.0259	.0240	.0249	.0257	.0278

model developed in section 5 of the Phase I, Segment 2 writeup.⁽³⁾ This model takes into account the effect of the water loss rate which is significant in Expt. 186.

A mass balance around the system pictured in Fig. 38 gives the following relation:

$$V \frac{d\bar{C}}{dt} = \dot{q}_T (C_{in} - \bar{C}) + \dot{q}_2 (1 - e^{-ka^* \tau_2^f}) (C^\infty - C_{in}) \quad (1)$$

where

$$C_{in} = \frac{\dot{q}_T - \dot{q}_{loss}}{\dot{q}_T} \bar{C} + \frac{\dot{q}_{loss}}{\dot{q}_T} C^M \quad (2)$$

V = total volume of all fracture flow paths = $V_1 + V_2$

V_2 = volume of hot region flow path

C^M = (SiO_2) makeup = concentration of SiO_2 in the makeup water

C^∞ = $(SiO_2^{sat})_{T=T_{max}}$ = saturation concentration of quartz at T_{max}

\bar{C} = $(\overline{SiO_2})$ = average concentration of SiO_2 at time t

k = dissolution mass transfer coefficient, cm/sec

a^* = rock surface area to fluid volume ration, cm^{-1}

\dot{q}_2 = fluid circulation rate through hot region at time t

\dot{q}_T = total fluid circulation rate at time t

$\dot{q}_{loss} = \dot{q}_{makeup}$ = fluid loss rate to permeation at time t

τ_2 = mean residence time in hot region = V_2 / \dot{q}_2

f = fraction of plug flow conversion = function of dispersion in hot region ($f \leq 1$)

SCHEMATIC OF FENTON HILL SYSTEM

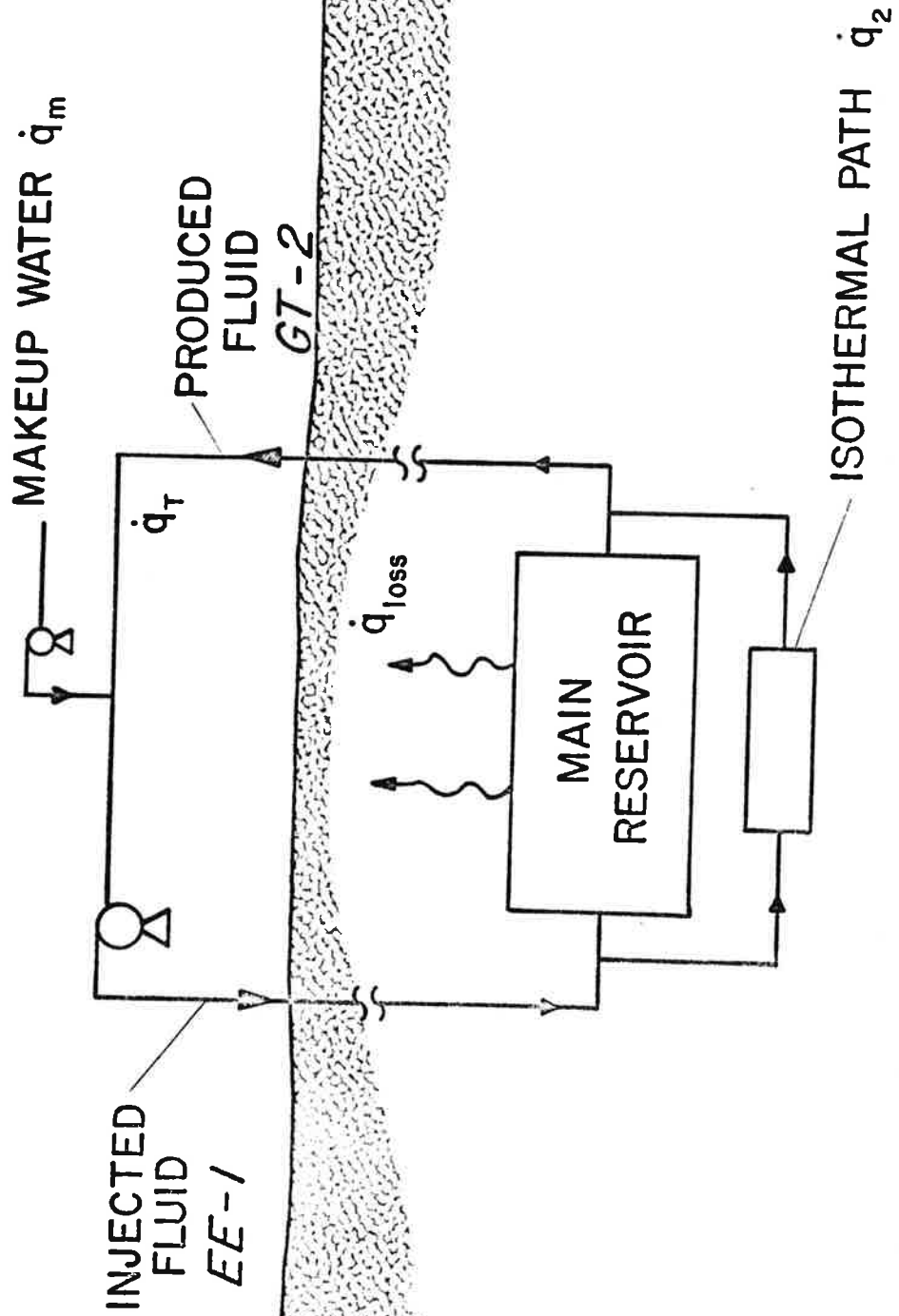


Figure 38. Idealized Reservoir System.



Substituting for C^{in} gives

$$V \frac{d\bar{C}}{dt} = \dot{q}_{1loss} (C^M - \bar{C}) + \dot{q}_2 (1 - e^{-\theta}) [C^\infty - \bar{C} + \frac{\dot{q}_{1loss}}{\dot{q}_T} (\bar{C} - C^M)] \quad (3)$$

where $\theta = ka\tau_2$.

rearranging

$$\dot{q}_2 = \frac{V \frac{d\bar{C}}{dt} + \dot{q}_{1loss} (\bar{C} - C^M)}{(1 - e^{-\theta}) [C^\infty - \bar{C} + \frac{\dot{q}_{1loss}}{\dot{q}_T} (\bar{C} - C^M)]} \quad (4)$$

where

$V = 10000$ gal from dye experiments

$\frac{d\bar{C}}{dt} = \text{Constant} = -1.17 \times 10^{-4}$ ppm/min

\dot{q}_{1loss} is taken from Fig. 25

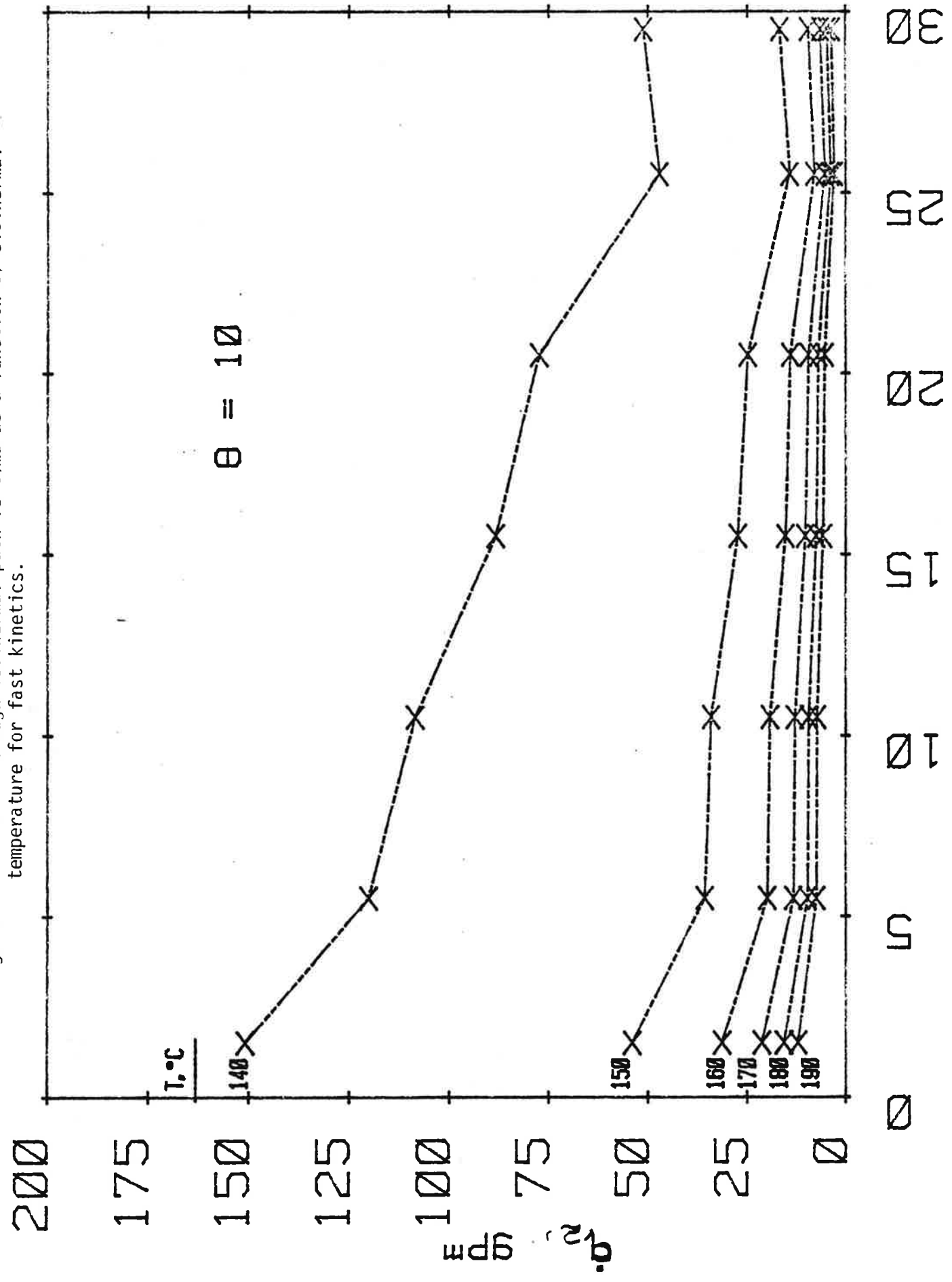
C^M is from Fig. 37

θ is taken to be large so $e^{-\theta} \rightarrow 0$

C^∞ is chosen to be the SiO_2 sat (qtz controlled) at the temperature of the hot region.

For large θ , the effect of kinetic dissolution rates is small and the change in concentration with time is due to mixing concentrated fluid with less concentrated fluid. As long as the concentration in the makeup fluid, C^M , is less than the average fluid concentration, \bar{C} , a high \dot{q}_{1loss} will strongly influence the change in concentration with time (eqn. 3). For an observed concentration vs time graph the value of \dot{q}_2 as a function of C^∞ (and therefore temperature) can be calculated using equation (4). A plot of \dot{q}_2 vs time as a function of isothermal temperature is given in Fig. 39. With the assumption

Fig. 39. Flow rate through isothermal path vs time as a function of isothermal temperature for fast kinetics.



of very fast kinetics in the isothermal path, the mixing model predicts that the flowrate through this path must decline from an initial 80 gpm to about 30 gpm at a temperature of 145°C. Lower temperature would require a higher flow rate as would slower kinetic rates of dissolution. At 140°C, the total flow rate is not sufficient to account for the buildup. As temperatures increase, the required flow rate drops and approaches 5-10 gpm for a temperature of 190°C. This is quite consistent with the results of the Phase I, Segment 2 test where the isothermal path temperature was $\sim 189^\circ\text{C}$ and the corresponding flow rate was ~ 4 gpm.

VIII. SUMMARY AND CONCLUSIONS

A. Thermal Drawdown Results

During this 28-day flow experiment, the GT-2B reservoir outlet temperature decreased from 136°C to 98°C. Due primarily to a slowly increasing GT-2B reservoir outlet pressure at a constant surface back-pressure level of 1400 psi, the GT-2 outflow slowly increased during this time interval from an initial value of about 100 gpm to a final value of about 150 gpm. Therefore, during Expt. 186, the reservoir thermal power ($E_{out} - E_{in}$) decreased only slightly, from an initial value of 1.54 MW(th) to a final value of 1.44 MW(th).

An effective heat transfer area (one side) of 8000 m² was found to match the drawdown data for this experiment. Since this is the same area as for the previous 75-day test, we can conclude that operation in the high back-pressure mode did not result in the hoped for large increase in heat extraction area.

However, as discussed later, a comparison of spinner surveys at high and low back pressure shows a significant shift downwards in the GT-2B fluid entry points for Expt. 186. These lower fracture outlets are presumably closer to the main EE-1 fracture inlet at 9050 ft, so that the flow-weighted mean reservoir outlet temperature profile during Expt. 186 should actually be lower than the theoretical curve for a 8000 m² fracture would indicate. Possibly, the effects of buoyancy are becoming apparent under this high back-pressure mode of operation. Some speculative calculations suggest that under these conditions, natural convection and viscous drag in

the fracture are approximately the same magnitude. In this case, natural convection may be contributing as much as 25% to the circulating fluid heat pickup.

B. Reservoir Specific Flow Impedance

This experiment has clearly demonstrated that the reservoir flow impedance is primarily a function of the downhole pressure at the fracture outlet. Under conditions of low back-pressure at GT-2, the reservoir flow impedance is large and concentrated near the fracture exit. However, this fracture-to-wellbore flow impedance drops almost linearly with increasing back-pressure at GT-2 until it essentially vanishes at or near the local reservoir value for S_3 . At this point, for the inlet flow conditions of Expt. 186, a "residual" reservoir flow impedance of about 0.4 psi/gpm remains, primarily concentrated near the EE-1 fracture inlet.

During Expt. 186, at a near-constant GT-2 back-pressure of 1400 psi, the downhole pressure at 8850 feet increased by about 200 psi as a result of the gradual cooling of the ascending column of fluid. In response to this increasing downhole pressure, the reservoir flow impedance dropped from a maximum value of 2.0 early in the experiment to a final value just under 0.5 psi/gpm.

From an analysis of the low back-pressure flow data from the 75-day Phase I test and Expt. 190, it is clear that the drop in reservoir flow impedance during the 75-day test represents a reversible phenomenon. Following Expt. 186, the measured low back-pressure reservoir flow impedance "recovered" to a value of 5.65 psi/gpm. Further, the decrease in the reservoir flow impedance during the 75-day test, from an initial value of 15 psi/gpm to a final value of about 3 psi/gpm, can be directly correlated

with the decrease in the reservoir outlet temperature during this test. Since the majority of the reservoir flow impedance for these conditions was concentrated at the fracture outlet, undoubtedly as a wellbore stress concentration, it is reasonable to conclude that thermal contraction stresses in this region -- a direct analog of pressurization -- probably accounted for the observed decrease in reservoir flow impedance with decreasing reservoir outlet temperature. That the Expt. 190 flow impedance of 5.65 psi/gpm at a reservoir outlet temperature of 105°C compares so closely with the 75-day Phase I reservoir flow impedance of 5.6 psi/gpm at a reservoir outlet temperature of 106°C supports this conclusion.

C. GT-2B Outlet Flow Redistribution Due to High Back-Pressure

Under conditions of high back-pressure at GT-2, the mean reservoir fluid entry point into the GT-2B wellbore shifts downwards by about 80 to 85 feet relative to the mean fluid entry point under low back-pressure flow conditions. This redistribution of flow is accounted for by the opening of a near-vertical fracture near the bottom of GT-2B, under a downhole pressurization level approaching the local value of S_3 .

The conductance of this near-vertical fracture-wellbore connection increased by a factor of 9.8 between low and high back-pressure conditions. This variation is close to that predicted by an empirical correlation based on extensive laboratory measurements of the variation of fracture permeability with confining stress. However, if this lowermost GT-2B flow connection was instead an intersecting high-angle joint dipping 65 to 70 degrees, the predicted increase in permeability would have been only about 1.3 to 2.5, much less than the observed permeability increase of almost ten.

Na-Fluorescein dye tracer studies conducted with high back-pressure at GT-2 have shown some important differences from those of run segment 2 of Phase I (75-day circulation test) with low backpressure at GT-2. Changes in the distribution of flow from production zones in GT-2B can be correlated with changes in the observed residence time distributions (RTD) with the majority of dispersion effects caused by a superposition of mixed flows in the GT-2B wellbore. The fracture system flowing volume under high back-pressure condition is somewhat smaller than that obtained at low back-pressure [median volumes of 13,000 vs 10,000 gal].

The following GT-2B flow connection model fits the observed data:

- A lowermost near-vertical fracture-wellbore intersection centered at a depth of about 8850 feet.
- A set of high-angle joints, dipping between 65 and 70 degrees, which intersect the wellbore between the depths of 8660 feet and 8800 feet.

D. Permeation Flow Analyses

With both EE-1 and GT-2 pressurized to a level approaching S_3 , the observed permeation and diffusion characteristics are generally those for the combined fracture systems. The diffusion parameter, $A\sqrt{KB/\beta_r}$, and long-term water losses reflect the properties of the fracture systems connected to both wellbores. The permeation flow in all phases of the experiment was approximately twice that measured during the 75-day flow test, with only EE-1 pressurized. However, due to flow bypass up the EE-1 annulus, the long-term water loss during Expt. 186 may actually have been quite similar to that during the 75-day flow test.

The source of the increasing water loss after the seventh day of Expt. 186 (9-25-78) was determined, during Expt. 190 to be an inlet flow bypass up the wellbore annulus outside the production casing string in EE-1. During Expt. 186, this bypass flow increased by about 25 gpm. However, following Expt. 190, this EE-1 bypass flow was measured at 40 gpm. Expt. 190 was terminated due to this problem.

E. Fluid Geochemistry

High makeup flow rates during Expt. 186 constantly diluted the fluid in the reservoir. Because of this high dilution, none of the dissolved species attained "steady state"; rather a very gradual decline in concentration with time was observed in all species. Due to the use of water from the GT-2 pond (which contained high TDS) for makeup water early in the experiment, there was an initial spike in the concentration-time curves. This spike had the effect of obscuring the change in fluid composition with time due to chemical interaction in the reservoir.

The silica vs time data were analyzed using the mixing model developed in Phase I, Segment 2 to set temperature and flow rate constraints on flow through a portion of the reservoir.

REFERENCES

1. Brown, D. and H. Murphy, "Procedure for High Back Pressure and Long-Term Pumping Experiments, Rev. 2 (Expt. 186)," G-3 Memorandum, July 24, 1978.
2. Albright, J., "Experiment 185 - Dresser Atlas Acoustic Attenuation With Flow Into EE-1 with GT-2 Shut In," G-3 Memorandum, July 13, 1978.
3. Tester, J. W. and J. N. Albright, eds., "Hot Dry Rock Energy Extraction Field Test: 75 Days of Operation of a Prototype Reservoir at Fenton Hill, Segment 2, Phase I," (LASL report to be published shortly).
4. Potter, R., "The Use of Radioactive Tracers in HDR Reservoir Studies," G-3/79/#5, March 28, 1979.
5. Brown, D. W., "GT-2A Pumping Tests: A Lesson in History," G-3/78/#34, Dec. 14, 1978.
6. Tester, J. W., G. E. Morris, R. G. Cummings, and R. L. Bivins, "Electricity from Hot Dry Rock Geothermal Energy: Technical and Economic Issues," LA-7603-MS and UC-66f, Jan. 1979.
7. Potter, R., "April 12, 1978 Spinner Survey of GT-2B," G-3/78/#6, April 17, 1978.
8. Jones, Frank O. Jr., "A Laboratory Study of the Effects of Confining Pressure on Fracture Flow and Storage Capacity in Carbonate Rocks," J. of Petr. Tech., Vol. 27, Jan. 1975.
9. LASL HDR Project Staff, "Hot Dry Rock Geothermal Energy Development Project," Los Alamos Scientific Laboratory Progress Report LA-7109-PR, Los Alamos, NM, 1977.
10. Fisher, H. N., "An Interpretation of the Pressure and Flow Data for the Two Fractures of the Los Alamos Hot Dry Rock (HDR) Geothermal System," Proc. of the 18th U.S. Symposium on Rock Mechanics, Keystone, Colorado, June 22, 1977.